Inorg. Chem. **2008**, *47*, 2994−3013

Novel Iron(III) Porphyrazine Complex. Complex Speciation and Reactions with NO and H_2O_2

Alexander Theodoridis,[†] Joachim Maigut,[†] Ralph Puchta,[†] Evgeny V. Kudrik,[†,‡] and Rudi van Eldik*[,†]

Inorganic Chemistry, Department of Chemistry and Pharmacy, University of Erlangen-Nürnberg, Egerlandstrasse 1, 91058 Erlangen, Germany, and University of Chemistry and Technology, Av. F. Engels 7, 153000 Ivanovo, Russia

Received October 15, 2007

The complex [iron(III) (octaphenylsulfonato)porphyrazine]$^{5-}$, Fe^{III}(Pz), was synthesized. The pK_a values of the axially coordinated water molecules were determined spectrophotometrically and found to be pK_{a_1} = 7.50 ± 0.02 and pK_{a_2} = 11.16 ± 0.06. The water exchange reaction studied by ^{17}O NMR as a function of the pH was fast at pH = 1, k_{ex} = (9.8 ± 0.6) × 10^6 s^{-1} at 25 °C, and too fast to be measured at pH = 10, whereas at pH = 13, no water exchange reaction occurred. The equilibrium between mono- and diaqua Fe^{III}(Pz) complexes was studied at acidic pH as a function of the temperature and pressure. Complex-formation equilibria with different nucleophiles (Br^- and pyrazole) were studied in order to distinguish between a five- (in the case of Br^-) or six-coordinate (in the case of pyrazole) iron(III) center. The kinetics of the reaction of Fe^{III}(Pz) with NO was studied as a model ligand substitution reaction at various pH values. The mechanism observed is analogous to the one observed for iron(III) porphyrins and follows an I_d mechanism. The product is (Pz)$Fe^{II}NO^+$, and subsequent reductive nitrosylation usually takes place when other nucleophiles like OH^- or buffer ions are present in solution. Fe^{III}(Pz) also activates hydrogen peroxide. Kinetic data for the direct reaction of hydrogen peroxide with the complex clearly indicate the occurrence of more than one reaction step. Kinetic data for the catalytic decomposition of the dye Orange II by H_2O_2 in the presence of Fe^{III}(Pz) imply that a catalytic oxidation cycle is initiated. The peroxide molecule first coordinates to the iron(III) center to produce the active catalytic species, which immediately oxidizes the substrate. The influence of the catalyst, oxidant, and substrate concentrations on the reaction rate was studied in detail as a function of the pH. The rate increases with increasing catalyst and peroxide concentrations but decreases with increasing substrate concentration. At low pH, the oxidation of the substrate is not complete because of catalyst decomposition. The observed kinetic traces at pH = 10 and 12 for the catalytic cycle could be simulated on the basis of the obtained kinetic data and the proposed reaction cycle. The experimental results are in good agreement with the simulated ones.

Introduction

Catalytic oxidation reactions have gained in interest in recent years. Their industrial significance has increased for several reasons. One is the production of stable and efficient oxidants such as dimethyldioxirane that can be easily prepared.[1] Another is that side products of industrial processes, such as dioxins and chlorinated phenols, have to be degraded in wastewater and the oxidant has to be reduced to environmentally friendly products.[2] Furthermore, the detergent industry is also interested in these processes and especially in their selectivity because tenacious stains have to be removed while at the same time the fabric should not be damaged. It is also important that stain removal takes place at low temperatures by avoiding chlorine-basedcompounds.[3] Because oxygen activation either is not applicable or requires catalysts of which the handling is very difficult,

* To whom correspondence should be addressed. E-mail: vaneldik@chemie.uni-erlangen.de.
† University of Erlangen-Nürnberg.
‡ University of Chemistry and Technology.

(1) (a) Baumstark, A. L.; Vasquez, P. C. *J. Org. Chem.* **1988**, *53*, 3437–3439. (b) Murray, R. W.; Gu, D. *J. Chem. Soc., Perkin Trans. 2* **1993**, 2203–2207. (c) Murray, R. W.; Singh, M.; Williams, B. L.; Moncrieff, H. M. *J. Org. Chem.* **1996**, *61*, 1830–1841.
(2) Gupta, S. S.; Stadler, M.; Noser, C. A.; Ghosh, A.; Steinhoff, B.; Lenoir, D.; Horwitz, C. P.; Schramm, K.-W.; Collins, T. J. *Science* **2002**, *296*, 326–328.

10.1021/ic702041g CCC: $40.75
Published on Web 03/20/2008

Scheme 1. (a) Three Groups of Porphyrinoid Systems and (b) the Complex $Fe^{III}(Pz)$[a]

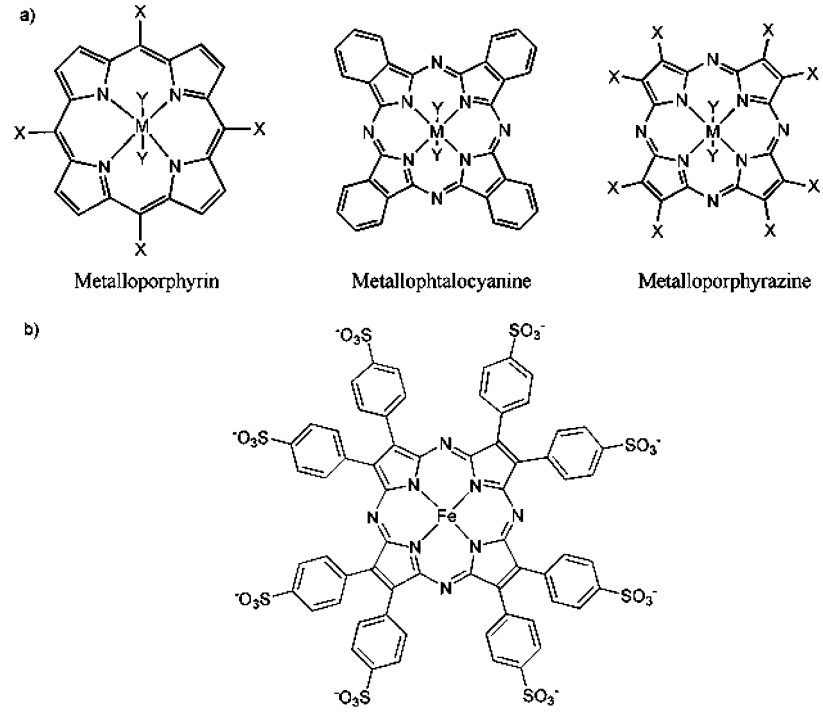

[a] The axial substituents (H_2O or OH^-) are not shown here. The Fe^{III} complex has an overall charge of 7− in the monoaqua form.

the activation of the green oxidant hydrogen peroxide has become important and the subject of many studies in recent years.[3a,4] The catalytic activities of a large variety of complexes consisting of different ligands (bidentate, tridentate, tetradentate, porphyrins, etc.) and metal centers such as iron or manganese have been tested.[3,4] The key step in all of these reactions is the coordination of the peroxide molecule to the metal center and the subsequent cleavage of the "activated" O−O bond. Spectator ligand tuning could lead to more effective catalysts and therefore to cheaper production steps in the industry.

Porphyrins have been utilized to activate dioxygen (viz., Cytochrome P450). Because iron(II) porphyrins are oxygen-sensitive, efforts focus on the catalysis of these reactions by starting with iron(II) porphyrins.[5,6] The direct reaction with peroxides produces the catalytic active species. The rate-determining step in these catalytic cycles is the cleavage of the peroxide O−O bond because coordination to the Fe^{III} center is usually substitution-controlled and a fast process. Homolytic cleavage produces an $OH^{\bullet}$ radical and a $(Por)Fe^{IV}{=}O$ species, whereas heterolytic cleavage results in the formation of a hydroxyl ion and $(Por^{\bullet+})Fe^{IV}{=}O$ (i.e., a porphyrin cation radical). The difference between the two oxidation states, i.e., $(Por)Fe^{IV}{=}O$ versus $(Por^{\bullet+})Fe^{IV}{=}O$, is of great importance because the first species can catalyze one-electron oxidation reactions, whereas the second species is able to catalyze two-electron oxidation steps such as the oxidation of *cis*-stilbene.[5] The generated radicals in the first case can also destroy the porphyrin ring or lead to a Fenton-like reaction.

Other macrocyclic systems have also been employed in these reactions. Iron porphyrazines and phthalocyanines are two large groups of compounds that are potential catalysts for oxidation reactions (Scheme 1).[7] However, only porphyrin complexes have been widely studied kinetically in the literature.[8] It has also been shown that phthalocyanine complexes can catalyze epoxidation reactions,[7] but the kinetics of such reactions have only been studied to a limited extent. On the other hand, as far as we know, no detailed study has been performed on iron(III) porphyrazines.

The three porphyrinoid complex groups in Scheme 1 are all macrocyclic systems with significant differences in the nature of the macrocycle. The *meso*-C atoms are substituted by N atoms when going from the porphyrin to the porphyrazine macrocycle. The electronegativity of the aza bridge is higher than that of the methine bridge, resulting in a more electronegative porphyrazine. The smaller-core size of Pz results in a larger σ-donor interaction that elevates the $d_{x^2-y^2}$ orbital, thereby contributing to the relative stability of the intermediate-spin state in $Fe^{III}(Pz)$.[9] However, the replacement of the *meso*-C atom by a N atom also has a large effect

(3) (a) Hage, R.; Lienke, A. *Angew. Chem.* **2006**, *118*, 212–229. (b) Hage, R.; Iburg, J. E.; Kerschner, J.; Koek, J. H.; Lempers, E. L. M.; Martens, R. J.; Racherla, U. S.; Russel, S. W.; Swarthoff, T.; van Vliet, M. R. P.; Warnaar, J. B.; van der Wolf, L.; Krijnen, B. *Nature* **1994**, *369*, 637–639.
(4) (a) Kryatov, S. V.; Rybak-Akimova, E. V.; Schindler, S. *Chem. Rev.* **2005**, *105*, 2175–2226. (b) Meunier, B.; de Visser, S. P.; Shaik, S. *Chem. Rev.* **2004**, *104*, 3947–3980. (c) Costas, M.; Mehn, M. P.; Jensen, M. P.; Que, L., Jr. *Chem. Rev.* **2004**, *104*, 939–986.
(5) Franke, A.; Hessenauer-Ilicheva, N.; Meyer, D.; Woggon, W.-D.; van Eldik, R. *J. Am. Chem. Soc.*. , in press.
(6) Woggon, W.-D. *Acc. Chem. Res.* **2005**, *38*, 127–136.
(7) Sorokin, A.; Meunier, B. *Eur. J. Inorg. Chem.* **1998**, 1269–1281.
(8) (a) Lane, B. S.; Burgess, K. *Chem. Rev.* **2003**, *102*, 3811–3836. (b) Denisov, I. G.; Makris, T. M.; Sligar, S. G.; Schlichting, I. *Chem. Rev.* **2004**, *104*, 903–938.
(9) Liao, M. S.; Scheiner, S. *J. Comput. Chem.* **2002**, *23*, 1391–1403.

on the size of the macrocycle in that the four pyrrole rings are "squeezed" together. Thus, the central metal ion has less space to occupy an "in-plane" position. This is especially important when it comes to the activation of small molecules like NO and peroxides by such complexes.

Porphyrazine complexes such as [Fe^{III}(Pz)] have a further advantage in that they have a high solubility in water that results from the deprotonation of the sulfonic acid groups and makes it possible to perform the studies in aqueous media (or mixtures of MeOH/water). In the reported work, changes in the pH proved to be crucial for the reactivity of the complex in both nucleophilic substitution reactions and the activation of small molecules such as NO and H_2O_2. In order to pinpoint the reactivity and the underlying reaction mechanisms of this new class of water-soluble porphyrazines, they should be investigated in terms of known reactions, viz., water exchange, activation of NO, and catalytic oxidation of Orange II, which have been previously studied for many porphyrin systems. The number of unknown parameters in the new system can in this way be minimized, for instance, in terms of the pattern of NO activation and subsequent reductive nitrosylation and degradation of Orange II. In the present study, we, therefore, investigated the reactivity of [Fe^{III}(Pz)] in water for the different reaction types mentioned. Further studies could also include the activation of peroxides in organic solvents, which would widen the scope of comparison with related non-water-soluble porphyrin complexes.

Experimental Section

Synthesis of the Iron(III) Porphyrazine Complex. (a) Synthesis of Octaphenylporphyrazineiron(III) [Fe(OPhPz)]. A total of 2 g (0.0087 mol) of diphenylfumaronitrile was dissolved in 30 mL of α-chloronaphthalene. The solution was dioxygenated with argon and heated to 210 °C. A total of 3.6 g (0.0184 mol) of iron pentacarbonyl (***Caution!*** *Forms flammable mixtures with air*) was added directly to the reaction mixture in 6 portions over a time period of 2 h. After additional heating (1 h) and cooling to room temperature, the mixture was diluted with 150 mL of diethyl ether and the red precipitate was filtered off and washed with methanol. The precipitate was dissolved in 60 mL of concentrated sulfuric acid, and the solution was poured into 200 mL of ice-cold water. The blue precipitate was filtered off and washed with water. After drying (6 h at 120 °C), the complex was washed with methanol in a Soxhlet apparatus. Yield: 1.47 g (69%). Calcd for $C_{64}H_{40}N_8Fe(OH)(H_2O)$: C, 75.96; H, 4.28; N, 11.07. Found: C, 75.44; H, 4.39; N, 10. 87.

(b) Synthesis of Iron(III) (Octa-*p*-sulfonatophenyl)-porphyrazine [Fe^{III}(Pz)]. A total of 1 g (10^{-3} mol) of Fe(OPhPz) was dissolved in 5 mL of chlorosulfonic acid, and the resulting mixture was stirred for 24 h at room temperature. The solution was poured into a cold saturated solution of NaCl (50 mL). The blue precipitate was filtered off, washed with water, and heated at 100 °C. The product was dissolved in 40 mL of distilled water and purified by column chromatography [Molselect G-25 (Hungary), eluent = water]. After evaporation, 0.98 g of product was obtained. The product was recrystallized from a 1 M $HClO_4$ solution. The water was evaporated, and the product was collected in the form of a dark-red powder. Unfortunately, we were unable to obtain single crystals of the complex. Calcd for $C_{64}H_{42}ClFeN_8O_{29}S_8$: C, 44.31; H, 2.44; N, 6.46; O, 26.74; S, 14.79. Found: C, 44.21; H, 2.46; N, 6.50; O, 26.8; S, 14.81.

Materials. All solutions were freshly prepared in distilled and purified water (Milli-Q system). A standard solution of H_2O_2 was purchased from Acros Organics (35% MW), the concentration of which was checked by titration with $KMnO_4$ in an acidic medium. $NaClO_4$ and triflic acid were of p.a. quality and were obtained from Acros Organics.

Orange II was purchased from Sigma-Aldrich and recrystallized from a water/ethanol mixture. The elemental analysis showed 99.9% purity (C, 54.8 (calcd 54.86); H, 3.11 (calcd 3.16); N, 8.03 (calcd 8.00); S, 9.07 (calcd 9.15). The absorbance coefficient ϵ has the value of 19 788 M^{-1} cm^{-1} at 484 nm and pH = 9.66. A pK_a value of 11.21 ± 0.01 was determined by spectrophotometric titration of a 10^{-4} M solution. The ϵ values at a specific pH and wavelength could then be calculated (see Figure S1, Supporting Information).

NO (Air Liquide) was purified by passing through an Ascarite II (Aldrich) and a P_2O_5 (Acros) column. Nitrite impurities in an acidic NO saturated solution could not be detected at 350 nm (characteristic band of nitrite with $\epsilon = 50$ M^{-1} cm^{-1}). $NaNO_2$ was of p.a. quality and was purchased from Acros.

General Procedures. The pH measurements were carried out with a WTW inoLab level 1 pH meter at constant temperature (25 °C). Stopped-flow measurements were performed on an Applied Photophysics SX-18 MV stopped-flow spectrophotometer. The solutions were rapidly mixed, and the kinetic trace was recorded at a single wavelength. At least 5 kinetic runs were recorded for each experimental condition. The values reported are the average of the measurements, and the deviation is the calculated standard deviation. The temperature was controlled with a Haake K20 thermostat with an accuracy of ±0.1 °C. For the repetitive scan measurements, a TIDAS J&M rapid-scan spectrophotometer was attached to the stopped-flow instrument. High-pressure stopped-flow experiments were performed at pressures up to 130 MPa on a custom-built instrument described before.[10] Electron paramagnetic resonance (EPR) spectra of solid samples were recorded on a JEOL JES-FA200 spectrometer. UV–vis spectra were recorded on a Varian 5G Cary spectrophotometer.

Solutions of NO were prepared by saturating the buffer with dinitrogen and then with NO in a gastight syringe. The desired concentration was achieved by diluting the saturated NO solution (1.8 mM at 25 °C) with an appropriate volume of a dinitrogen-saturated buffer solution. The thermostat bath of the stopped-flow machine was also saturated with dinitrogen to prevent traces of oxygen from entering the flow lines. The NO solutions were found to be stable in the syringes of the stopped-flow instrument at temperatures above 10 °C for more than 20 min.

Kinetic traces for the direct reaction of the iron(III) porphyrazine complex with H_2O_2 were fitted to a double-exponential function with the *Origin 7.5* program, as well as with the Applied Photophysics software package. The results were the same in each case. The kinetic traces of the catalytic reaction had to be fitted to a single-exponential function with steady state, i.e., the mixed first- and zero-order function in eq 1,

$$A_t = at + Ae^{-kt} \quad (1)$$

where a is the slope of the linear zero-order reaction, t is time, A is the absorbance change during the first-order reaction, k is the

(10) (a) van Eldik, R.; Palmer, D. A.; Schmidt, R.; Kelm, H. *Inorg. Chim. Acta* **1981**, *50*, 131–135. (b) van Eldik, R.; Gaede, W.; Wieland, S.; Kraft, J.; Spitzer, M.; Palmer, D. A. *Rev. Sci. Instrum.* **1993**, *64*, 1355–1357.

observed rate constant of the first-order reaction, and A_t is the absorbance at time t.

Iron(III) porphyrazine solutions were prepared by dilution of a standard aqueous solution (10^{-3} M) in the appropriate quantity of a buffer solution. Hydrogen peroxide solutions were prepared by dilution of a standard 35% H_2O_2 solution. Because H_2O_2 is a weak acid, the pH of every nonbuffered solution had to be adjusted by the dropwise addition of a degassed concentrated NaOH solution. Orange II solutions were prepared by dilution of a standard Orange II solution (10^{-2} M) in the appropriate buffer solution. For the study of the catalytic cycle, appropriate amounts of the iron(III) porphyrazine and Orange II standard solutions were added to the buffer.

NMR Experiments. The water exchange rate on $Fe^{III}(Pz)$ and the corresponding activation parameters were studied by the ^{17}O NMR line-broadening technique.[11] Aqueous solutions (540 μL) of $Fe^{III}(Pz)$ were prepared at pH = 1 (triflic acid), pH = 10 (0.1 M CAPS buffer), and pH = 13 (0.1 M NaOH). A total of 60 μL of enriched ^{17}O-labeled water (normalized 10% ^{17}O-labeled H_2O, Deutero) was added to the solutions. A reference sample was prepared by adding the same amount of enriched ^{17}O-labeled water to the corresponding aqueous solution (pH = 1, 10, and 13) without the addition of $Fe^{III}(Pz)$. Variable-temperature and -pressure Fourier transform ^{17}O NMR spectra were recorded at a frequency of 54.24 MHz on a Bruker Advance DRX 400WB spectrometer. A home-made high-pressure probe[12] was used for the variable-pressure experiments performed at pH = 1.

The line-broadening data as function of the temperature and pressure were treated with the Swift and Connick equation as reported elsewhere.[13–15] The value of k_{ex}^0 obtained from the plot of $\ln(k_{ex})$ versus P by extrapolation to atmospheric pressure was in good agreement with the corresponding value of k_{ex}^0 from the temperature-dependent measurements at ambient pressure.

Results and Discussion

Titration of $Fe^{III}(Pz)$. $Fe^{III}(Pz)$ was titrated spectrophotometrically as a function of the pH. The measurement was started at acidic pH ($HClO_4$ and CF_3SO_3H were used for acidification of the solution), and small drops of a concentrated NaOH solution were added so that the volume change was kept minimal. The spectrum of the resulting solution at each pH was measured in a cuvette. The absorbance at different wavelengths was plotted versus the pH, and the data in Figure 1 could be fitted to a double-sigmoidal function (eq 2).

$$\mathrm{Abs} = A_1 + \frac{A_1 - A_2}{1 + e^{(\mathrm{pH} - \mathrm{p}K_{a_1})/d(\mathrm{pH})}} + \frac{A_2 - A_3}{1 + e^{(\mathrm{pH} - \mathrm{p}K_{a_2})/d(\mathrm{pH})}} \quad (2)$$

In this equation, A_1, A_2, and A_3 are the absorbance values of the dominating species at each pH. The resulting pK_a values of the complex are $\mathrm{p}K_{a_1} = 7.50 \pm 0.02$ and $\mathrm{p}K_{a_2} = 11.16 \pm 0.06$. The titration was repeated by starting with a pH = 12 solution and adding concentrated $HClO_4$. The spectral changes and the final result were exactly the same, demonstrating that the observed changes are fully reversible. The first pK_a value is accompanied by very large spectral changes. These changes are unusual if the only reaction observed is the deprotonation of the axially bound water molecules. Because large spectral changes usually indicate either redox activity or a change in the spin state in macrocyclic chemistry, this suggests that the observed UV–vis spectral changes occur because of a spin-state change of the Fe^{III} center. According to the literature,[16] UV–vis spectra of five- and six-coordinate iron(III) phthalocyanines differ significantly. The five-coordinate iron(III) porphyrazines are stabilized in the unusual $^3/_2$ spin state, i.e., intermediate spin state, contrary to the iron(III) porphyrins, where the six-coordinate diaqua species is the dominating one at low pH. The reasons for this difference can be found in the nature of the macrocycle. The *meso*-N bridges of the porphyrazine ring are smaller than the C bridges of the porphyrin. This leads to the displacement of the Fe center out of the plane in the absence of strong nucleophiles in solution. Furthermore, the N atoms lead to a higher basicity of the molecule; i.e., the molecule is a better σ donor and π acceptor. The addition of a base to an acidic solution causes the coordination of a

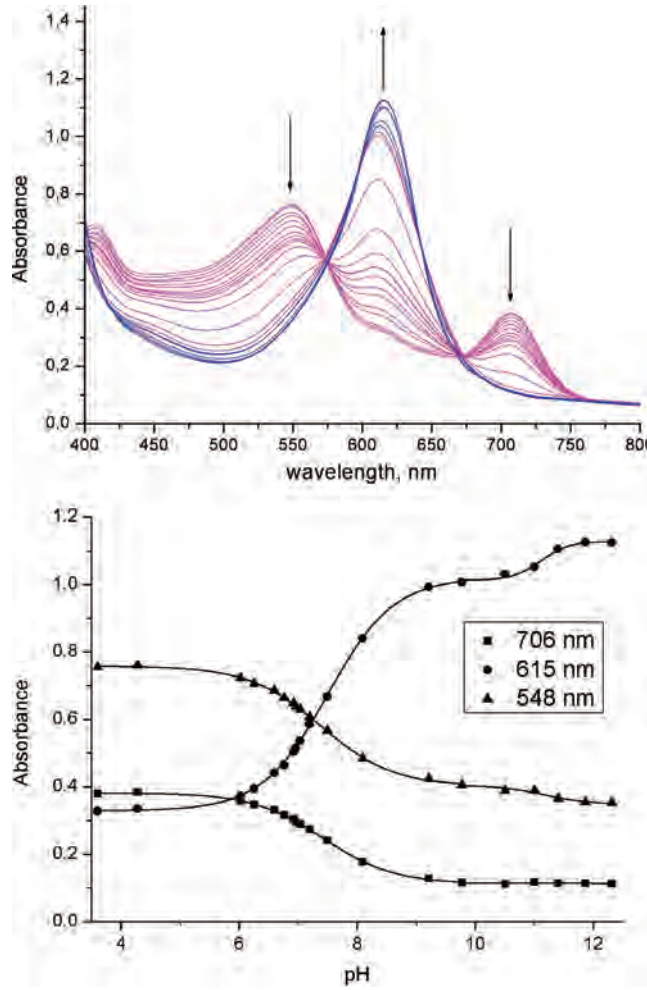

Figure 1. Spectral changes recorded during the pH titration of $Fe^{III}(Pz)$ and the fits obtained with eq 2 at three different wavelengths.

(11) Schneppensieper, T.; Zahl, A.; van Eldik, R. *Angew. Chem., Int. Ed.* **2001**, *40*, 1678–1680.
(12) Zahl, A.; Neubrand, A.; Aygen, S.; van Eldik, R. *Rev. Sci. Instrum.* **1994**, *65*, 882–886.
(13) (a) Swift, T. J.; Connick, R. E. *J. Chem. Phys.* **1962**, *37*, 307. (b) Swift, T. J.; Connick, R. E. *J. Chem. Phys.* **1964**, *41*, 2553–2554.
(14) Bloembergen, N. J. *Chem. Phys.* **1957**, *27*, 595–596.
(15) Newman, K. E.; Meyer, F. K.; Merbach, A. E. *J. Am. Chem. Soc.* **1979**, *101*, 1470–1476.
(16) Stuzhin, P. A.; Hamdush, M.; Ziener, U. *Inorg. Chim. Acta* **1995**, *236*, 131–139.

Scheme 2. Deprotonation of the Fe^{III}(Pz) Complex[a]

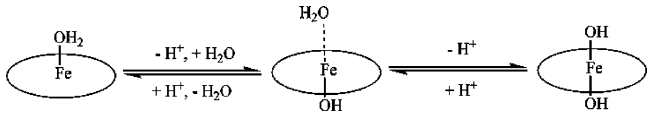

[a] Only the axial ligands (H_2O or OH^-) of the proposed complexes are shown in more detail.

Scheme 3. Possible Dimerization of Fe^{III}(Pz)

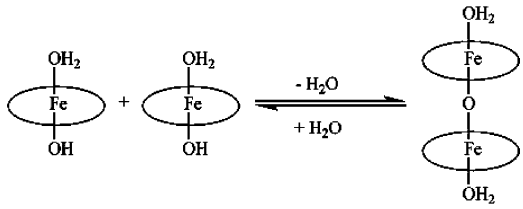

hydroxo ligand, an effect that forces the Fe center into the macrocyclic plane. This coordination change leads to a spin-state change from $^3/_2$ to $^1/_2$. A comparison of spectra found in the literature[16] with those in Figure S2 in the Supporting Information(spectra of Fe^{III}(Pz) at pH = 3 and 10) shows good agreement. Futhermore, in the spectrum at pH = 10, the Soret and Q bands are located at almost the same position as those at pH = 12, which means that there is no spin-state change between the two pH values. This is the first indication that in the pH range 1−6 the monoaqua Fe^{III}(Pz) species is present in solution, whereas at higher pH, six-coordinate Fe^{III} species are formed, as suggested in Scheme 2.

At higher pH, the sixth ligand (water in this case) is expected to be very labile as a result of the trans effect of the hydroxo ligand. Furthermore, we investigated whether the aquahydroxo complex could dimerize at around pH = 9. The dimerization process should depend on the concentration of Fe^{III}(Pz), as suggested by Scheme 3. Spectra were recorded for different Fe^{III}(Pz) concentrations and then divided by the Fe^{III}(Pz) concentration.

All spectra resulted in the same absorbance value for the Soret band at the same position, from which we conclude that dimerization at low complex concentrations cannot play a significant role. This is supported by the fact that the porphyrazine ligand has an overall charge of 8−, which apparently hinders dimerization due to electrostatic repulsion. According to this information, the second pK_a value, which is accompanied by small spectral changes, represents the deprotonation of the aqua ligand to form the six-coordinate dihydroxo-Fe^{III}(Pz) species.

^{17}O NMR Experiments. At pH = 1, the water exchange data could be fitted to the Swift and Connick[13] equation. Table S1 in the Supporting Information reports the line widths measured at each temperature for the reference and Fe^{III}(Pz) samples. Figure 2 shows the temperature dependence of $\ln(1/T_{2r})$. The water exchange rate was calculated to be $(9.8 \pm 0.6) \times 10^6$ s^{-1} at 298 K. This value is within the range of that reported for anionic porphyrin complexes of

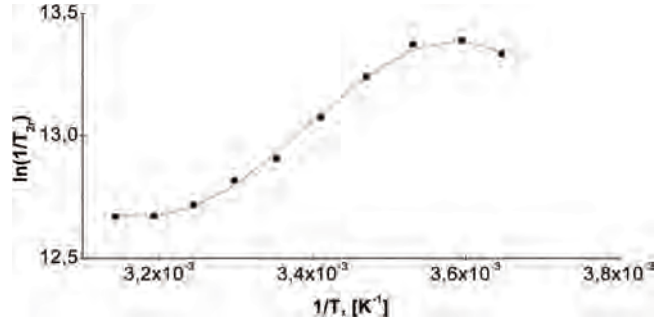

Figure 2. Kinetic data for the water exchange reaction at pH = 1. [Fe^{III}(Pz)] = 8 mM; [^{17}O-labeled H_2O] = 0.55 M (60 μL of a 600 μL solution).

Fe^{III}.[17] Contrary to the iron porphyrins, where the water exchange mechanism is clearly dissociative, the value of $\Delta S^{\ddagger}$ for water exchange on $[Fe^{III}(Pz)(H_2O)]^{7-}$ is much smaller (viz., $\Delta H^{\ddagger} = 37 \pm 2$ kJ mol^{-1}, $\Delta S^{\ddagger} = +13 \pm 7$ J mol^{-1} K^{-1}). The pressure dependence of the reaction (Figure S3 in the Supporting Information) also indicates a dissociative interchange character ($\Delta V^{\ddagger} = +0.9 \pm 0.1$ and $+1.0 \pm 0.1$ cm^3 mol^{-1}). These results can be compared to those of iron(III) porphyrin systems.[18] It is known that the Fe^{III} center is stabilized in a spin admixed state in acidic solutions, is located in the plane of the porphyrin macrocycle, and is six-coordinate with two axially bound water molecules. The water exchange mechanism was found to be strongly dissociative; i.e., first the coordinated water molecule has to leave the coordination sphere, after which the entering water molecule binds to the Fe^{III} center. The significantly different values found for the activation parameters ($\Delta S^{\ddagger}$ and $\Delta V^{\ddagger}$) in the present study support the suggestion that the Fe center of the $[Fe^{III}(Pz)]^{7-}$ molecule is five-coordinate. In the case of a six-coordinate Fe^{III} center, much larger and more positive values would be expected, as in the case of the iron(III) porphyrins.[17] The small and positive values of the activation parameters $\Delta S^{\ddagger}$ and $\Delta V^{\ddagger}$ clearly demonstrate that the five-coordinate Fe^{III} center remains in the intermediate-spin state. If a spin-state change occurred and the Fe center would be six-coordinate in the transition state with two water molecules bound axially, the transition from an intermediate- to low-spin state would be reflected in much larger and more negative activation parameters. This suggests that the axial water molecule is displaced at the same side of the porphyrazine macrocycle.

At pH = 10, only a very fast water exchange reaction could be observed (see Figure 3 and Table S2 in the Supporting Information). The rate is too fast to be measured such that the error in the fit of the data is also very large. This is consistent with labilization of the axially bound water molecule due to the trans effect of the hydroxide ion bound in the sixth coordination site. It is reasonable to expect a longer bond distance for the $Fe-OH_2$ bond due to the trans influence of the hydroxo ligand, which should have a shorter bond to the metal center.

(17) Jee, J.-E.; Eigler, S.; Hampel, F.; Jux, N.; Wolak, M.; Zahl, A.; Stochel, G.; van Eldik, R. *Inorg. Chem.* **2005**, *44*, 7717–7731.
(18) Hoshino, M.; Laverman, L.; Ford, P. C. *Coord. Chem. Rev.* **1999**, *187*, 75–102.

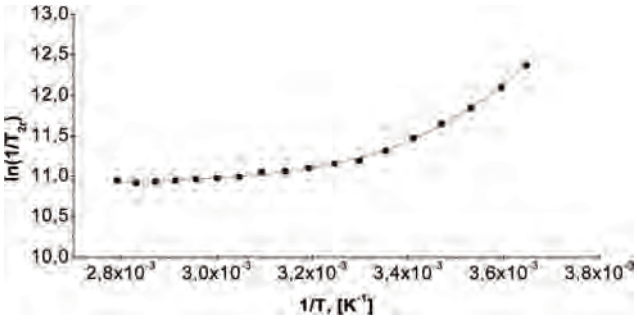

Figure 3. Kinetic data for the water exchange reaction at pH = 10. The reaction is too fast and the errors are too large for accurate data to be extracted. [Fe^{III}(Pz)] = 8 mM, [^{17}O-labeled H_2O] = 0.55 M (60 μL of a 600 μL solution).

Scheme 4. Coordination of a Second Water Molecule to Five-Coordinate Fe^{III}(Pz)(H_2O)

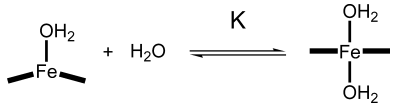

Finally, no water exchange reaction could be observed at pH = 13. This is in agreement with the prediction that at this pH only the very inert dihydroxo complex is present in solution. The hydroxide anion is a much stronger nucleophile than water, and its displacement should be very unfavorable.

Pressure- and Temperature-Dependent UV–Vis Spectra. The rate of the water exchange reactions and the reported activation parameters are in agreement with the reactions described in Scheme 2. The large absorbance changes in the UV–vis spectra as a function of the pH correspond not only to the deprotonation of one water molecule but also to the coordination of an additional sixth ligand to the five-coordinate Fe^{III} center (at low pH) and its transformation from an intermediate-spin state to a low-spin state. On the other hand, the small absorbance changes observed for the second acid dissociation step are consistent with the deprotonation of the second water molecule. However, one cannot exclude the existence of an equilibrium between a mono- and diaqua complex at low pH as proposed in Scheme 4.

If this equilibrium really exists in solution, there should be observable UV–vis spectral changes as a function of the temperature and pressure. Therefore, UV–vis spectra were recorded as a function of the pressure (see Figure S4 in the Supporting Information). On going from low (5 MPa) to high (150 MPa) pressure, an increase in the intensity of the band at 616 nm is observed. The increase is characteristic of the generation of a low-spin species (see spectra in Figure 1). This means that the equilibrium shown in Scheme 4 is shifted to the right at elevated pressure and an additional water molecule is coordinated. From the absorbance at each pressure, it was possible to calculate the equilibrium constant, *K*. The intermediate-spin state of Fe^{III}(Pz) does not exhibit a band at 616 nm, and it was therefore possible to calculate the concentrations of the intermediate- and low-spin Fe^{III}(Pz) species from the difference in the absorbance of this band.

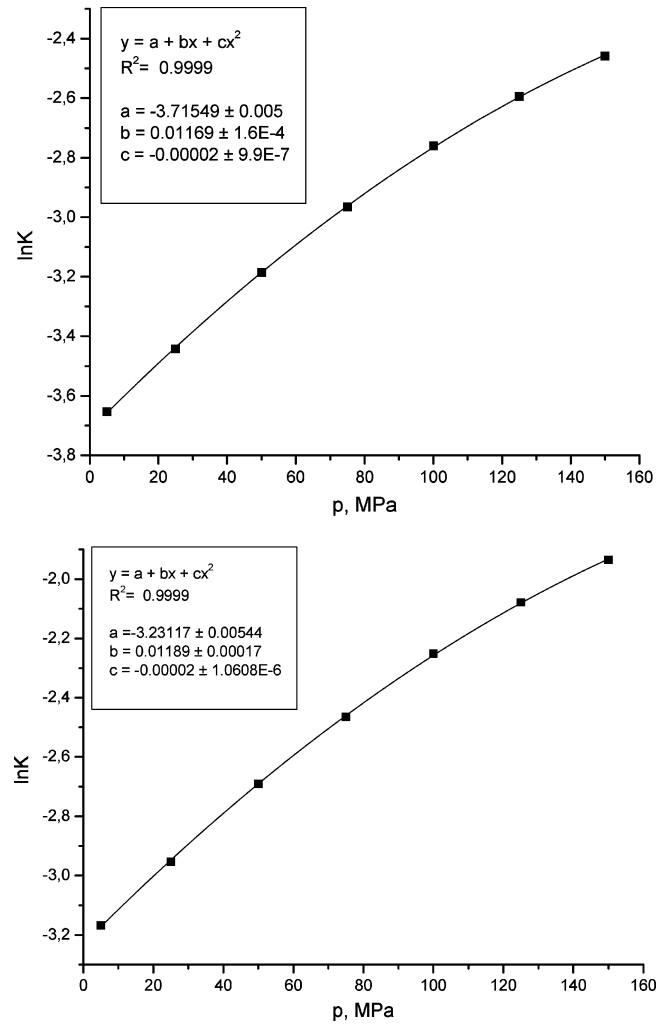

Figure 4. Plots of ln *K* versus pressure. In the top diagram, *K* was calculated using ϵ = 32 000 M^{-1} cm^{-1} and in the lower diagram ϵ = 20 000 M^{-1} cm^{-1} (see also Table S3 in the Supporting Information). The calculated reaction volumes are $\Delta V^\circ = -29.0 \pm 1.0$ cm^3 mol^{-1} (top diagram) and -29.5 ± 1.0 cm^3 mol^{-1} (lower diagram).

The reaction volume, ΔV°, could then be calculated according to eq 3,[19]

$$\ln K = a - \frac{\Delta V^\circ}{RT}p + cp^2 \qquad (3)$$

where *K* is the equilibrium constant for the reaction in Scheme 4, *p* the pressure in MPa, *T* the temperature, and *R* the gas constant. For this calculation, the extinction coefficient of the diaqua, low-spin species at 616 nm must be known in order to estimate the equilibrium constant at each pressure. Because this is presently unknown, we used the ϵ value of the aquahydroxo complex, which is expected to be very close. To demonstrate that this assumption is not very critical, we also calculated the *K* values on the basis that ϵ is 2×10^4 M^{-1} cm^{-1} instead of 3.2×10^4 M^{-1} cm^{-1}, i.e., 30% smaller (see Table S3 in the Supporting Information). In both cases, the results were almost identical (see Figure 4) and independent of ϵ, viz., $\Delta V^\circ = -29.0 \pm 1.0$ and -29.5

(19) van Eldik, R. *Inorganic High Pressure Chemistry—Kinetics and Mechanisms*; Elsevier Publications: Amsterdam, The Netherlands, 1986.

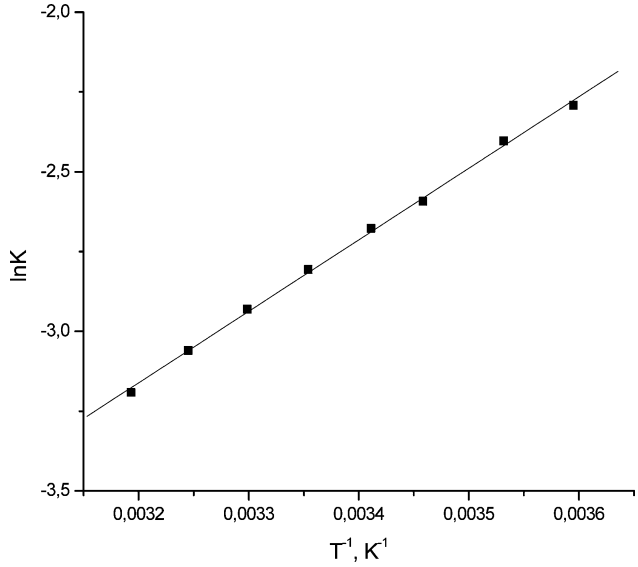

Figure 5. Plot of ln K versus T^{-1} for the coordination of one water molecule to the five-coordinate $[Fe^{III}(Pz)(H_2O)]^{7-}$ to produce the low-spin six-coordinate $[Fe^{III}(Pz)(H_2O)_2]^{7-}$.

$\pm$ 1.0 cm^3 mol^{-1} for $\epsilon = 3.2 \times 10^4$ and 2×10^4 M^{-1} cm^{-1}, respectively. The very negative reaction volume is consistent with the sum of two contributions, viz., the coordination of the additional water molecule in the coordination sphere of the iron porphyrazine molecule and the change in the spin state from intermediate to low spin, both for which a volume collapse is expected. The coordination of a water molecule causes a volume collapse of ca. -13 cm^3 mol^{-1}.[20] The transition from high- to low-spin Fe^{III} is accompanied by a volume collapse of between -12 and -15 cm^3 mol^{-1}.[21] Therefore, the experimental reaction volume of ca. -30 cm^3 mol^{-1} supports that the observed spectral changes correspond to a shift in the equilibrium to the right, as shown in Scheme 4.

The temperature dependence of the UV–vis spectrum is reported in Figure S5 in the Supporting Information. When the temperature is decreased from 40 to 5 °C, an increase in the intensity of the band at 616 nm is observed. This means that the equilibrium in Scheme 4 is shifted to the blue, low-spin complex (i.e., to the right side of the equilibrium). Again from the spectral changes we could determine the value of the equilibrium constant K at each temperature and plot ln K versus T^{-1}, as is done in Figure 5 (data are given in Table S4 in the Supporting Information). From the linear fit of the data, we could calculate $\Delta H°$ and $\Delta S°$ according to eq 4, which were found to be -18.6 ± 0.3 kJ mol^{-1} and -86 ± 1 J K^{-1} mol^{-1}, respectively. The negative reaction enthalpy shows

$$\ln K = \frac{\Delta S°}{R} - \frac{\Delta H°}{RT} \qquad (4)$$

that the reaction as written is exothermic. More information can be obtained from the large and negative reaction entropy. Again, the sum of the two contributions mentioned above account for the very negative value. Despite the existence of this equilibrium in solution, the dominant species at low pH is the red-colored, intermediate-spin, five-coordinate $[Fe^{III}(Pz)(H_2O)]^{5-}$ species. Even at high pressure and low temperature, the equilibrium constant K is very small (see Table S3 in the Supporting Information).

EPR Spectroscopy. The EPR spectrum of crystalline $[Fe^{III}(Pz)(H_2O)]ClO_4$ was recorded (see Figure S6 in the Supporting Information). Similar spectra have been observed for five-coordinate Fe^{III} complexes, where the Fe^{III} center is in the intermediate-spin state ($S = {}^3/_2$).[22–24] In the absence of a strong nucleophile, the axial ligand of the Fe^{III} center is a water molecule. The signals at $g = 2$ and 4 are according to the literature characteristic of this spin state of the Fe center.

Theoretical Calculations. Because the crystal structure of $[Fe^{III}(Pz)(H_2O)]ClO_4$ is not known, we tried to calculate the structures of the $Fe^{III}(Pz)$ complexes as a function of the pH. We performed B3LYP/LANL2DZp hybrid density functional theory calculations, i.e., with pseudopotentials on the heavy elements and the valence basis set augmented with polarization functions.[25,26] In addition, the resulting structures were characterized as minima by computation of vibrational frequencies, and the wave function was tested for stability. The *Gausssian* suite of programs was used.[27]

To simplify the calculations, we neglected the *p*-sulfonatophenyl groups and included only the macrocycle with

(20) Richens, D. T. *Chem. Rev.* **2005**, *105*(6), 1961–2002.
(21) Binstead, R. A.; Beattie, J. K. *Inorg. Chem.* **1986**, *25*, 1481–1484.
(22) Niarchos, D.; Kostikas, A.; Simopoulos, A.; Coucouvanis, D.; Piltingsrud, D.; Coffman, R. E. *J. Chem. Phys.* **1978**, *69*, 4411–4418.
(23) Kerber, W. D.; Ramdhanie, B.; Goldberg, D. P. *Angew. Chem., Int. Ed.* **2007**, *46*, 3718–3721.
(24) Simkhovic, L.; Goldberg, I.; Gross, Z. *Inorg. Chem.* **2002**, *41*, 5433–5439.
(25) (a) Becke, A. D. *J. Phys. Chem.* **1993**, *97*, 5648–5652. (b) Lee, C.; Yang, W.; Parr, R. G. *Phys. Rev. B* **1988**, *37*, 785–789. (c) Stephens, P. J.; Devlin, F. J.; Chabalowski, C. F.; Frisch, M. J. *J. Phys. Chem.* **1994**, *98*, 11623–11627. (d) Dunning, T. H., Jr.; Hay, P. J. *Mod. Theor. Chem.* **1976**, *3*, 1–28. (e) Hay, P. J.; Wadt, W. R. *J. Chem. Phys.* **1985**, *82*, 270–283. (f) Hay, P. J.; Wadt, W. R. *J. Chem. Phys.* **1985**, *82*, 284–298. (g) Hay, P. J.; Wadt, W. R. *J. Chem. Phys.* **1985**, *82*, 299–310. (h) Huzinaga, S. *Gaussian Basis Sets for Molecular Calculations*; Elsevier: Amsterdam, The Netherlands, 1984.
(26) (a) The performance of the computational level employed in this study is well documented. For example, see: Puchta, R.; Meier, R.; van E. Hommes, N. J. R.; van Eldik, R. *Eur. J. Inorg. Chem.* **2006**, 4063–4067. (b) Scheurer, A.; Maid, H.; Hampel, F.; Saalfrank, R. W.; Toupet, L.; Mosset, P.; Puchta, R.; van E. Hommes, N. J. R. *Eur. J. Org. Chem.* **2005**, 2566–2574. (c) Illner, P.; Zahl, A.; Puchta, R.; van E. Hommes, N.; Wasserscheid, P.; van Eldik, R. *J. Organomet. Chem.* **2005**, *690*, 3567–3576. (d) Weber, C. F.; Puchta, R.; van E. Hommes, N.; Wasserscheid, P.; van Eldik, R. *Angew. Chem.* **2005**, *117*, 6187–6192. (e) Weber, C. F.; Puchta, R.; van E. Hommes, N.; Wasserscheid, P.; van Eldik, R. *Angew. Chem., Int. Ed.* **2005**, *44*, 6033–6038.
(27) Frisch, M. J.; Trucks, G. W.; Schlegel, H. B.; Scuseria, G. E.; Robb, M. A.; Cheeseman, J. R.; Montgomery, J. A., Jr.; Vreven, T.; Kudin, K. N.; Burant, J. C.; Millam, J. M.; Iyengar, S. S.; Tomasi, J.; Barone, V.; Mennucci, B.; Cossi, M.; Scalmani, G.; Rega, N.; Petersson, G. A.; Nakatsuji, H.; Hada, M.; Ehara, M.; Toyota, K.; Fukuda, R.; Hasegawa, J.; Ishida, M.; Nakajima, T.; Honda, Y.; Kitao, O.; Nakai, H.; Klene, M.; Li, X.; Knox, J. E.; Hratchian, H. P.; Cross, J. B.; Adamo, C.; Jaramillo, J.; Gomperts, R.; Stratmann, R. E.; Yazyev, O.; Austin, A. J.; Cammi, R.; Pomelli, C.; Ochterski, J. W.; Ayala, P. Y.; Morokuma, K.; Voth, G. A.; Salvador, P.; Dannenberg, J. J.; Zakrzewski, V. G.; Dapprich, S.; Daniels, A. D.; Strain, M. C.; Farkas, O.; Malick, D. K.; Rabuck, A. D.; Raghavachari, K.; Foresman, J. B.; Ortiz, J. V.; Cui, Q.; Baboul, A. G.; Clifford, S.; Cioslowski, J.; Stefanov, B. B.; Liu, G.; Liashenko, A.; Piskorz, P.; Komaromi, I.; Martin, R. L.; Fox, D. J.; Keith, T.; Al-Laham, M. A.; Peng, C. Y.; Nanayakkara, A.; Challacombe, M.; Gill, P. M. W.; Johnson, B.; Chen, W.; Wong, M. W.; Gonzalez, C.; Pople, A. *Gaussian 03*, revision C.02; Gaussian, Inc.: Wallingford, CT, 2004.

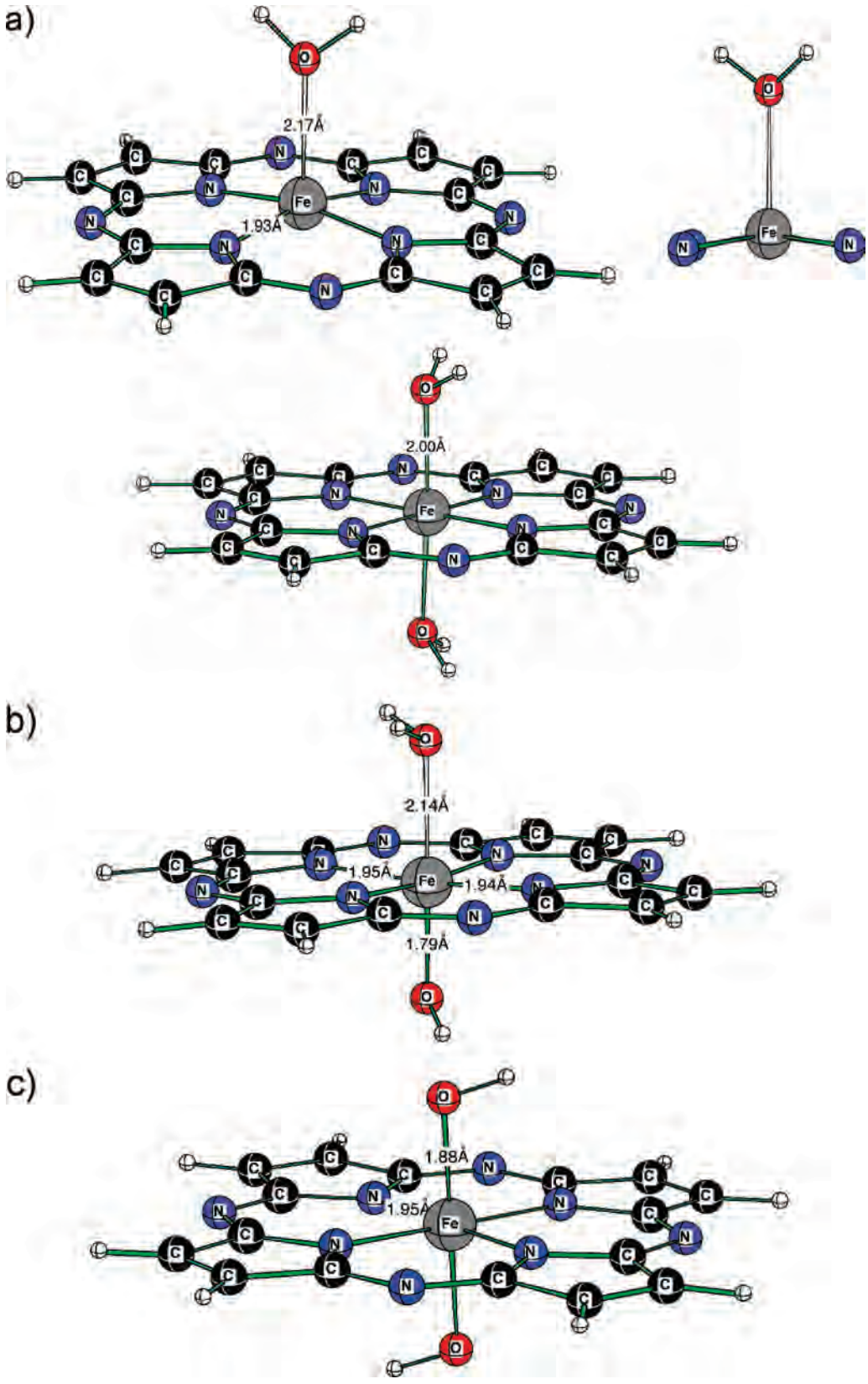

Figure 6. Calculated structures for the different species generated at different pH values: (a) mono- and diaqua complexes at acidic pH; (b) aquahydroxo complex at pH = 10; (c) dihydroxo complex at pH > 12.

the Fe^{III} center. The UB3LYP/LANL2DZp-G03 method was used. All four structures could be optimized, i.e., mono- and diaqua species, one aquahydroxo species, and one dihydroxo species. The calculated structures are reported in Figure 6.

At acidic pH, both structures are possible, viz., the intermediate-spin state $Fe^{III}(Pz)(H_2O)$ and the low-spin state $Fe^{III}(Pz)(H_2O)_2$. Both species are stable and show similar energies. The gas-phase calculation (B3LYP/LANL2DZp)

Scheme 5. Reaction of $[Fe^{III}(Pz)(H_2O)]^{5-}$ with Bromide

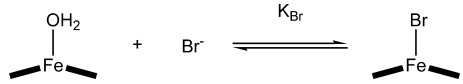

shows that the diaqua complex is more stable than the monoaqua complex ($\Delta E = -2.6$ kcal mol^{-1}). However, it is expected that additional factors like entropic and solvent effects will decrease the total energy for the monoaqua species.[28–32] For the diaqua species, the calculation shows that both water molecules have the same distance to the Fe^{III} center. However, as shown by the reported UV–vis spectra, the diaqua complex coexists only in low concentrations. The smaller pocket of the macrocycle forces the Fe^{III} atom to move "out of the plane", which will hinder coordination of the second water molecule.

At pH = 10, only the aquahydroxo species is formed. The water molecule is labilized by the trans effect of the hydroxo group. This is very well reflected by the distances of the water O atom and the hydroxo O atom to the Fe center (viz., 2.14 and 1.79 Å, respectively). The iron−water bond is therefore labilized, which is reflected in the larger bond distance. The Fe center is now low-spin and "in-plane" because the hydroxo group is a strong nucleophile and can force the Fe center to move "in-plane".

The structure at very alkaline pH is similar to that at pH = 10. In this case, the Fe center is axially coordinated by two hydroxides. Their distances to the Fe center are identical and equal to 1.88 Å, which is longer than that in the case of the aquahydroxo species. This can be accounted for in terms of the alternating trans influence of the two coordinated hydroxides. However, this bond distance is significantly shorter than the Fe−O distance in the mono- and diaqua complexes at low pH. These model calculations support the structural suggestions made in Schemes 2 and 4.

Titration with Weak and Strong Nucleophiles. Water can be considered to be a relatively weak nucleophile. To support the hypothesis that the transition from intermediate to low spin is not only pH-dependent but also ligand-dependent, the $[Fe^{III}(Pz)(H_2O)]^{5-}$ complex was titrated with bromide as a weak nucleophile and with pyrazole as a strong nucleophile. Figure S7 in the Supporting Information reports the spectral changes observed upon the addition of bromide to a solution of $[Fe^{III}(Pz)(H_2O)]^{5-}$. The overall reaction is given in Scheme 5.

The absorbance at different wavelengths was plotted as a function of the added bromide concentration (Figure S7 in the Supporting Information), and the data could be fitted to eq 5,

$$\mathrm{Abs} = A_0 + \frac{A_\infty K_{\mathrm{Br}}[\mathrm{Br}^-]}{1 + K_{\mathrm{Br}}[\mathrm{Br}^-]} \qquad (5)$$

where A_0 and A_∞ represent the absorbance at 0 and 100% conversion, respsectively, of $[Fe^{III}(Pz)(H_2O)]^{7-}$. The value

Scheme 6. Reaction of $[Fe^{III}(Pz)(H_2O)]^{7-}$ with Two Molecules of Pyrazole

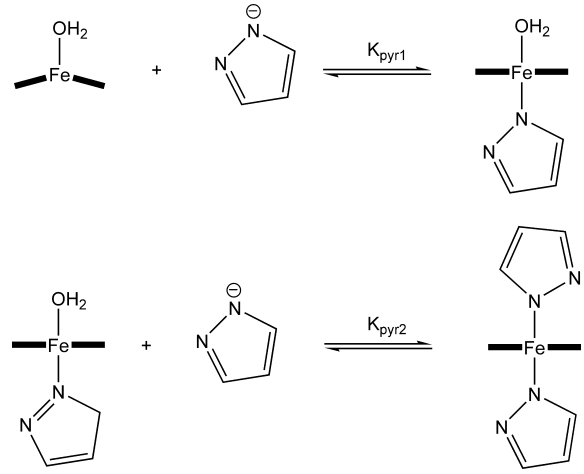

of K_{Br} was calculated from a nonlinear least-squares fit of the data to eq 5 and was found to be 1.2 ± 0.1 M^{-1}. The observed spectral changes indicate that only one bromide anion coordinates to the Fe^{III} center, which is further confirmed by the clean isosbestic points in the UV–vis spectra reported in Figure S7 in the Supporting Information.

In the titration of $[Fe^{III}(Pz)(H_2O)]^{7-}$ with pyrazole, the color of the solution changed to blue as indicated by the spectral changes reported in Figure S8 in the Supporting Information. No clean isosbestic points were observed. The increase in the band at 616 nm indicates the generation of a low-spin species upon the addition of an excess of pyrazole. The absorbance was plotted against the negative logarithm of the pyrazole concentration, and the data points could be fitted to eq 2. In this case, the values of pK_{a_1} and pK_{a_2} were replaced by pK_{pyr_1} and pK_{pyr_2} (see Scheme 6). Figure S8 in the Supporting Information presents the nonlinear least-squares fit to eq 2. The pK_{pyr_1} and pK_{pyr_2} values were found to be 3.5 ± 0.1 and 2.7 ± 0.1, respectively, such that $K_{pyr_1} = 3630 \pm 220$ M^{-1} and $K_{pyr_2} = 501 \pm 22$ M^{-1}. It is reported in the literature that strong donors like methylimidazole can change the spin state of the central Fe^{III} atom from the intermediate- to low-spin state.[33] Weak ligands, on the other hand, favor a five-coordinate Fe^{III} center.[33]

Reaction with NO. The ligand substitution reactions with pyrazole and bromide as nucleophiles were too fast to follow kinetically. Therefore, we investigated the kinetics of the substitution of coordinated water by NO as a representative substitution process. It is well-known that iron(III) porphyrins react with NO to form $(P)Fe^{II}NO^+$ as the product.[17] In this reaction, the Fe center is formally reduced whereas the NO

(28) Puchta, R.; Galle, M.; van E. Hommes, N.; Pasgreta, E.; van Eldik, R. *Inorg. Chem.* **2004**, *43*, 8227–8229.
(29) Hanauer, H.; Puchta, R.; Clark, T.; van Eldik, R. *Inorg. Chem.* **2007**, *46*, 1112–1122.
(30) Puchta, R.; van E. Hommes, N.; van Eldik, R. *Helv. Chim. Acta* **2005**, *88*, 911–922.
(31) Pasgreta, E.; Puchta, R.; Galle, M.; van E. Hommes, N.; Zahl, A.; van Eldik, R. *Chem. Phys. Chem.* **2007**, *8*, 1315–1320.
(32) Pasgreta, E.; Puchta, R.; Zahl, A.; van Eldik, R. *Eur. J. Inorg. Chem.* **2007**, 1815–1822.
(33) Fitzgerald, J. P.; Haggerty, B. S.; Rheingold, A. L.; May, L.; Brewer, G. A. *Inorg. Chem.* **1992**, *31*, 2006–2013.

Scheme 7. Reaction of Iron(III) Porphyrins with NO in the Presence of Another Nucleophile

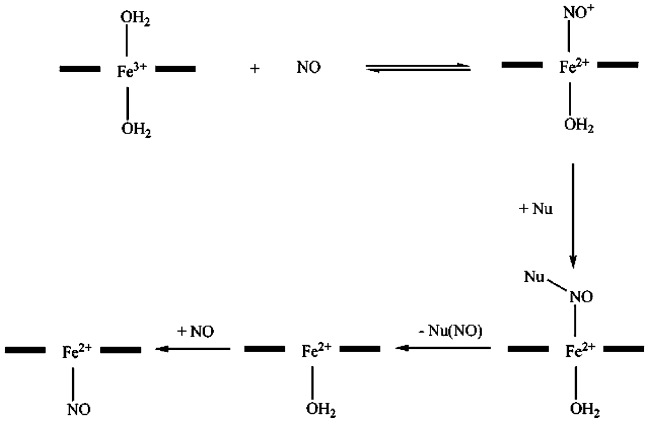

Scheme 8. Expected Reactions of $Fe^{III}(Pz)$ with NO at pH = 1 (a), 10 (b), and 12.4 (c)

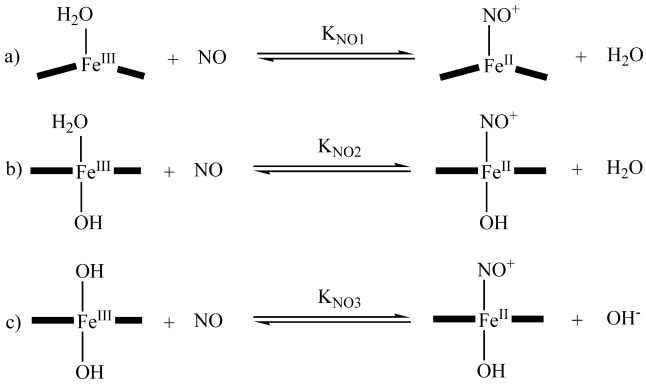

molecule is oxidized.[34,35] In addition, the product $(P)Fe^{II}NO^+$ can react with nucleophiles (Nu) such as NO_2^-, OH^-, and buffer anions, followed by the release of the addition product NuNO and the reaction of the reduced $(P)Fe^{II}$ species with NO to form $(P)Fe^{II}NO^{\bullet}$, as shown in Scheme 7.[17,34]

According to the results reported above, the $Fe^{III}(Pz)$ complex is present in different forms in the three selected pH ranges. At pH = 1, the monoaqua species $[Fe^{III}(Pz)(H_2O)]^{7-}$ is mainly present in solution. At pH = 10 and 12.4, the dominant species are the low-spin six-coordinate aquahydroxo and dihydroxo complexes, $[Fe^{III}(Pz)(H_2O)(OH)]^{8-}$ and $[Fe^{III}(Pz)(OH)_2]^{9-}$, respectively. All three species react with NO, and the reaction rate, as well as the activation parameters, offers mechanistic insight into the substitution behavior of the different $Fe^{III}(Pz)$ complexes. Scheme 8 summarizes the expected reactions for the interaction of $Fe^{III}(Pz)$ with NO in the three pH ranges. Tables S5−S7 in the Supporting Information summarize the observed rate constants for these reactions as a function of the NO concentration, temperature, and pressure. The pseudo-first-order rate constants k_{obs} depend linearly on the NO concentration at every pH.

(34) Theodoridis, A.; van Eldik, R. *J. Mol. Cat. A: Chem.* **2004**, *224*, 197–205.

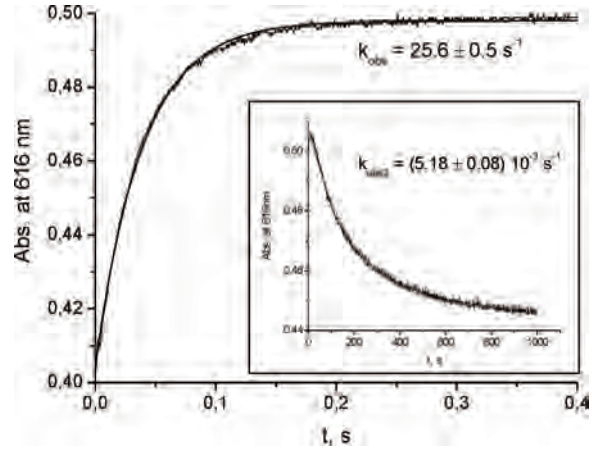

Figure 7. Kinetic trace and single-exponential fits of the two subsequent reactions observed upon mixing of $[Fe^{III}(Pz)(H_2O)(OH)]^{8-}$ with NO at 15 °C. [NO] = 5.8×10^{-4} M, μ = 0.2 M ($NaClO_4$), $[Fe^{III}(Pz)(H_2O)(OH)]^{8-}$] = 3×10^{-5} M, and pH = 10 (CAPS buffer).

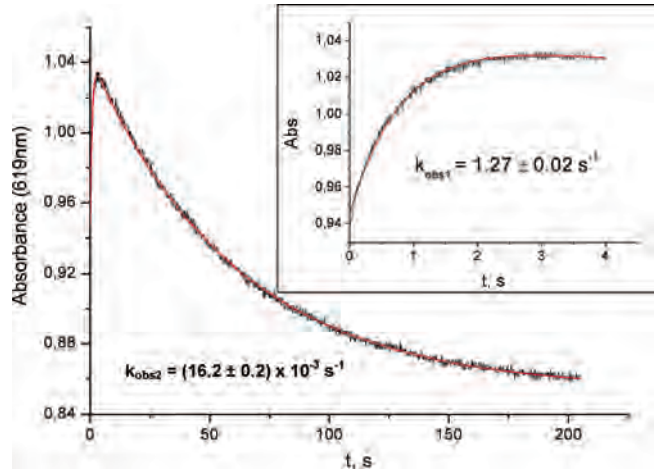

Figure 8. Kinetic trace and double-exponential fit of the first and second reaction steps of $[Fe^{III}(Pz)(OH)_2]^{9-}$ with NO. Inset: The first 4 s of the kinetic trace and its fit. [NO] = 1.8×10^{-4} M, μ = 0.7 M ($NaClO_4$), T = 10 °C, $[Fe^{III}(Pz)(OH)_2^{9-}]$ = 3×10^{-5} M, and pH = 12.4.

At pH = 1, the reaction with NO is very fast and its concentration dependence could only be studied at 278 K over a limited concentration range. A single first-order reaction step was observed under these conditions. The slope of the linear fit of the data in Figure S9 in the Supporting Information gives $k_{on} = (141 \pm 5) \times 10^3$ M^{-1} s^{-1} and the intercept $k_{off} = 5 \pm 2$ s^{-1}. The equilibrium constant K_{NO_1} equals $k_{on}/k_{off} = (29 \pm 10) \times 10^3$ M^{-1} at pH = 1 and 278 K.

At pH = 10 and 12.4, two reaction steps were observed. Typical kinetic traces recorded under these conditions are reported in Figures 7 and 8, respectively. Only the first step depended on the NO concentration. Upon the addition of nitrite or buffer, no change in the rate constant was observed. The second reaction step, however, was found to be very sensitive to changes in the nitrite and buffer concentration, which implies that the second reaction step involves the reaction of nitrite or buffer ions as nucleophiles with the positively charged, coordinated NO^+ ion, as outlined in Scheme 7. Figure S10 in the Supporting Information shows

(35) Wolak, M.; van Eldik, R. *J. Am. Chem. Soc.* **2005**, *127*, 13312–13315.

Scheme 9. Reactions of $Fe^{III}(Pz)$ with NO and the Proposed Transition States as a Function of the pH

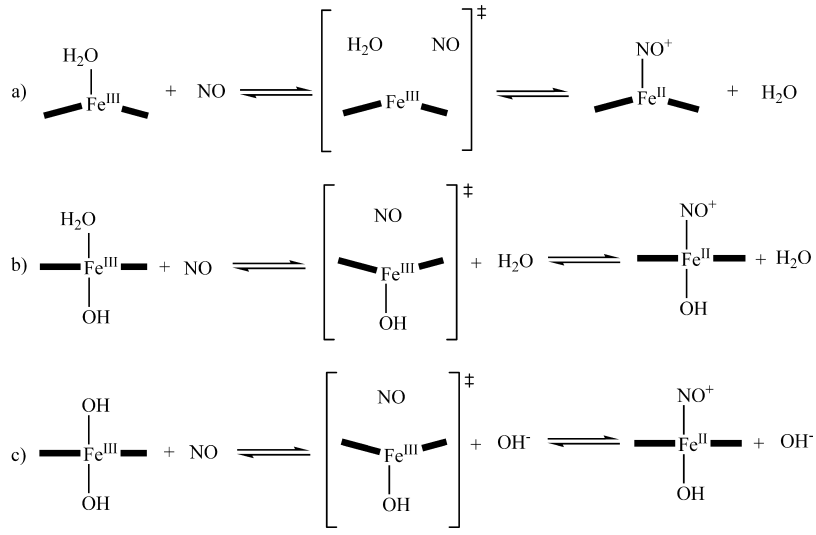

the dependence of k_{obs} on the NO concentration at different temperatures for the reaction at pH = 10. The reaction is slower than that at pH = 1, and no meaningful intercept is observed. At 25 °C, $k_{on} = (101 \pm 4) \times 10^3\ M^{-1}\ s^{-1}$. The activation parameters were calculated from a linear fit of the Eyring plot for k_{on} in Figure S11 in the Supporting Information, viz., $\Delta H^{\ddagger} = 56.5 \pm 0.8$ kJ mol^{-1} and $\Delta S^{\ddagger} = +40 \pm 3$ J K^{-1} mol^{-1}. The pressure dependence of k_{obs} was linear (see Figure S12 in the Supporting Information), from which it follows that $\Delta V^{\ddagger} = +13 \pm 1$ cm^3 mol^{-1}.

At pH = 12.4, the NO concentration dependence of the first reaction step showed a large intercept and a slower "on" reaction (see Figure S13 in the Supporting Information). A linear fit resulted in $k_{on} = (5.0 \pm 0.3) \times 10^3\ M^{-1}\ s^{-1}$ and $k_{off} = 9.1 \pm 0.2\ s^{-1}$ at 25 °C. From the temperature dependence of the reaction, $\Delta H^{\ddagger} = 100 \pm 7$ kJ mol^{-1} and $\Delta S^{\ddagger} = +165 \pm 22$ J K^{-1} mol^{-1} for the "on" reaction (Figure S14 in the Supporting Information) and $\Delta H^{\ddagger} = 76 \pm 3$ kJ mol^{-1} and $\Delta S^{\ddagger} = +31 \pm 16$ J K^{-1} mol^{-1} for the "off" reaction (Figure S15 in the Supporting Information). The activation volume for the "off" reaction was measured at a low NO concentration and found to be $+23 \pm 1$ cm^3 mol^{-1} (Figure S16 in the Supporting Information).

The results for the formation of the nitrosyl ($Fe^{II}NO^+$) complexes can be compared directly with the results of the ^{17}O-labeled H_2O exchange experiments. At pH = 1, a very fast water exchange reaction was observed in agreement with the very fast reaction observed with NO under these conditions. At pH = 10, the reaction with NO should be even faster on the basis of the water exchange data. However, this is not the case and the reaction is indeed much slower. This can only mean that under these conditions displacement of the coordinated water molecule is not the rate-determining step. Because the coordinated water molecule is very labile due to the trans effect of the hydroxyl ligand, this probably involves the formation of a five-coordinate $[Fe^{III}(Pz)(OH)]^{8-}$ intermediate. The subsequent reaction with NO to form the Fe−NO bond could be the rate-determining step because it is accompanied by a reduction of the Fe center and a change in the spin state. This is known to be the case for the binding of NO to iron(III) porphyrins at higher pH.[35] At pH = 12.4, where the dominant species is the dihydroxo complex, a 20 times slower reaction was observed. The Fe−OH bond strength controls the accessibility of the Fe^{III} center. Attack of the Fe center by NO is therefore inhibited and controlled by the slow dissociation of OH^-. The NO concentration dependence in Figure S13 in the Supporting Information exhibits large intercepts, indicating that the back-reaction (substitution of NO by hydroxide) is relatively fast under these pH conditions as a result of the trans effect of coordinated hydroxide. Scheme 9 represents the proposed mechanisms for the reaction with NO as a function of the pH.

Table S8 in the Supporting Information summarizes the rate and activation parameters for the reaction with NO at pH = 10 and 12.4. At pH = 10, k_{on} is ca. 20 times faster than that at pH = 12.4, in line with the higher lability of the aquahydroxo complex. The positive values of the activation entropy and activation volume for the "on" reaction at pH = 12 indicate the operation of a dissociative interchange (I_d) mechanism. This is in line with the expected lability of the water molecule trans to the hydroxide group that will induce a dissociative ligand interchange process. However, at pH = 12.4, the activation enthalpy and entropy for the "on" reaction are even more positive than those at pH = 10, indicating that NO coordination is controlled by the dissociation of the Fe−OH bond. The very positive activation volume for the "off" reaction at pH = 12.4 points to dissociative release of NO under the influence of the *trans*-hydroxo ligand, accompanied by a spin change from a low-spin (diamagnetic) $Fe^{II}NO^+$ complex to an intermediate- or high-spin transition state, as was recently reported for reactions of related iron(III) porphyrin complexes at high pH.[18]

Activation of H_2O_2. In order to study the activation of H_2O_2 by the different $[Fe^{III}(Pz)]$ complexes present in solution

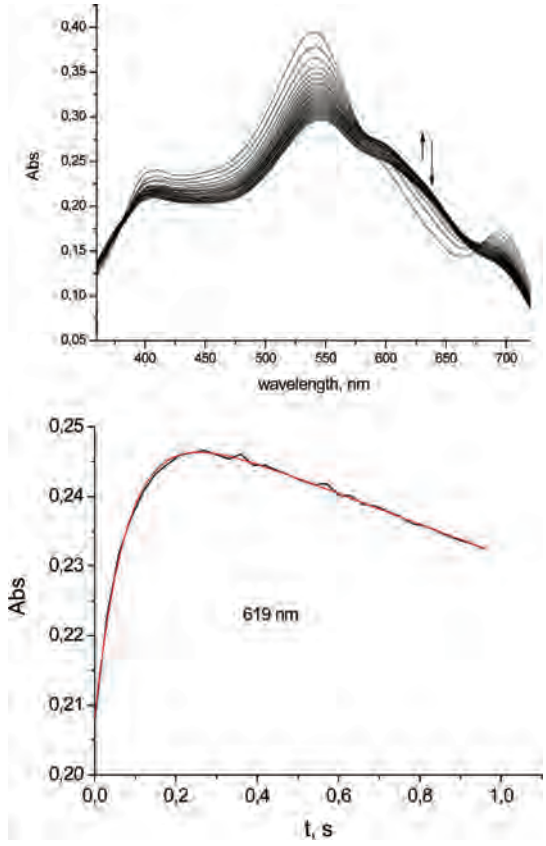

Figure 9. Spectral changes and the kinetic trace at 619 nm observed for the direct reaction of H_2O_2 with $[Fe^{III}(Pz)(H_2O)]^{7-}$. pH = 3, μ = 0.1 M ($NaClO_4$), T = 276 K, $[Fe^{III}(Pz)(H_2O)^{7-}] = 3 \times 10^{-5}$ M, and $[H_2O_2] = 3 \times 10^{-4}$ M. The kinetic trace was fitted with a double-exponential function.

Scheme 10. Structure of Orange II

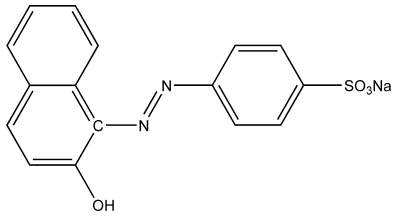

as a function of the pH, it turned out to be useful to first study the direct reaction of the different complexes with the oxidant, H_2O_2, and subsequently the oxidation of a substrate, Orange II in the present study (see Scheme 10), by H_2O_2 in the presence of the complex as the catalyst. From a combination of the two approaches, conclusions regarding the catalytic mechanism could be drawn. The decomposition of the Orange II dye is rather difficult to achieve in the absence of a suitable catalyst. At high pH values, it can be oxidized directly by peroxides, but the reaction is very slow. At low pH, Orange II is stable in the presence of strong oxidants like H_2O_2. Therefore, it is useful to study the oxidation of this dye with H_2O_2 in the presence of $Fe^{III}(Pz)$ as the catalyst.

The direct reaction of $[Fe^{III}(Pz)(H_2O)]^{7-}$ with H_2O_2 was studied at pH = 3. Figure 9 reports the observed spectral changes and the kinetic trace recorded at 619 nm for the

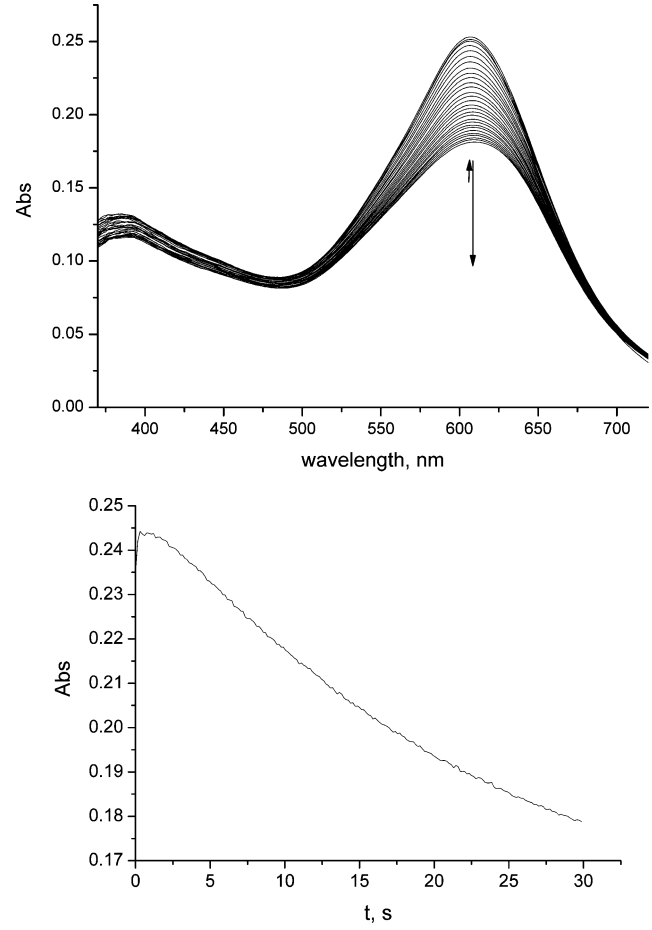

Figure 10. Typical spectral changes (Δt = 1.05 s) and the kinetic trace for the direct reaction of H_2O_2 with $[Fe^{III}(Pz)(H_2O)(OH)]^{8-}$. $[Fe^{III}(Pz)(H_2O)(OH)^{8-}] = 1.5 \times 10^{-5}$ M, $[H_2O_2] = 6 \times 10^{-4}$ M, pH = 10, T = 3 °C, and μ = 0.2 M ($NaClO_4$).

reaction of H_2O_2 with $[Fe^{III}(Pz)(H_2O)]^{7-}$ at pH = 3 and 3 °C. From the observed spectral changes and the rate of the reaction, some preliminary conclusions can be drawn. The first, fast reaction step can be assigned to the formation of the catalytically active species and the second, slower reaction to the decomposition of the porphyrazine. Because the first reaction step is very fast, we conclude that the reaction of H_2O_2 with $[Fe^{III}(Pz)(H_2O)]^{7-}$ is controlled by the water exchange reaction, as was also found for the reaction with NO. As in the case of NO, H_2O_2 binds to the Fe center at the same site as the coordinated water molecule according to a dissociative interchange mechanism.

For the direct reaction of $[Fe^{III}(Pz)(H_2O)(OH)]^{8-}$ with H_2O_2 at pH = 10, the spectral changes of the first reaction were too small to be able to measure any kinetic data (see Figure 10). This is probably due to the extremely fast substitution of the axially bound water molecule by hydrogen peroxide, and only the slow subsequent decomposition reaction can be observed.

Figure 11 shows the spectral changes and the kinetic trace at 619 nm for the reaction of $[Fe^{III}(Pz)(OH)_2]^{9-}$ with OOH^- (pK_a of H_2O_2 is 11.3) at pH = 12. Experiments at pH = 13 (see further discussion) indicated no reactivity of the complex anymore, suggesting that it is not the dihydroxo complex that is the reactive species but rather the much more labile

aquahydroxo complex that is present in ca. 12% at pH = 12 (pK_{a_2} = 11.2). The kinetic traces were fitted with a two-exponential function in line with the suggestion that the first reaction (increase in the absorbance at 619 nm) represents the rapid generation of the catalytically active complex, followed by the slow decomposition of the porphyrazine. The dependence of the pseudo-first-order rate constant for the first reaction on the HOO^- concentration is reported in Figure 12 (and Table S9 in the Supporting Information) as a function of the temperature. This data can be interpreted in terms of the reversible formation of the peroxo complex (Pz)FeOOH by the aquahydroxo complex as shown in Scheme 11, for which the rate law is given in eq 6.

$$k_{obs} = k_{off} + \frac{k_{on}[H^+][OOH^-]}{K_{a_2} + [H^+]} \qquad (6)$$

The slope and intercept of the linear fit of the data at 25 °C in Figure 12 were found to be 745 ± 31 M^{-1} s^{-1} and 0.27 ± 0.05 s^{-1}, respectively, and represent the terms $k_{on}[H^+]/(K_{a_2} + [H^+])$ and k_{off}, respectively, according to eq 6. From these values, the equilibrium constant K ($=k_{on}/k_{off}$) was found to be (2.2 ± 0.5) × 10^4 M^{-1}. The activation enthalpies and entropies for k_{on} and k_{off} could be calculated from the slopes of the linear fits (Figure 13), viz., $\Delta H^{\ddagger}_{on}$ = 74 ± 4 kJ mol^{-1} and $\Delta S^{\ddagger}_{on}$ = +76 ± 13 J K^{-1} mol^{-1}, and the intercepts, viz., $\Delta H^{\ddagger}_{off}$ = 53 ± 5 kJ mol^{-1} and $\Delta S^{\ddagger}_{off}$ = −77 ± 17 J K^{-1} mol^{-1}, respectively. The activation entropies for the "on" and "off" reactions suggest that the displacement of coordinated water in the aquahydroxo complex by OOH^- is controlled by the dissociation of water, whereas the back-reaction (displacement of coordinated OOH^- by water) must on the principle of microscopic reversibility be controlled by the dissociation of OOH^-, which involves charge creation that will increase electrostriction and account for the more negative activation entropy. Following the formation of (Pz)FeOOH, decomposition of the porphyrazine occurs in the subsequent slow reaction because it is generally known that such high oxidation species are unstable in water. In addition, they can also react with peroxide to produce oxygen and water via disproportionation of peroxide.

Catalytic Decomposition of Orange II by H_2O_2 in the Presence of $[Fe^{III}(Pz)(H_2O)]^{7-}$. The uncatalyzed decomposition of Orange II in the presence of H_2O_2 is very slow and strongly depends on the pH as shown by some typical kinetic traces summarized in Figure S17 in the Supporting Information. At low pH in the presence of $Fe^{III}(Pz)$, where the dominant species is $[Fe^{III}(Pz)(H_2O)]^{7-}$, Orange II is decomposed within a few seconds, as shown in Figure 14. The kinetic traces under these conditions indicate that the extent of decomposition of Orange II is proportional to the catalyst concentration employed. For example, when

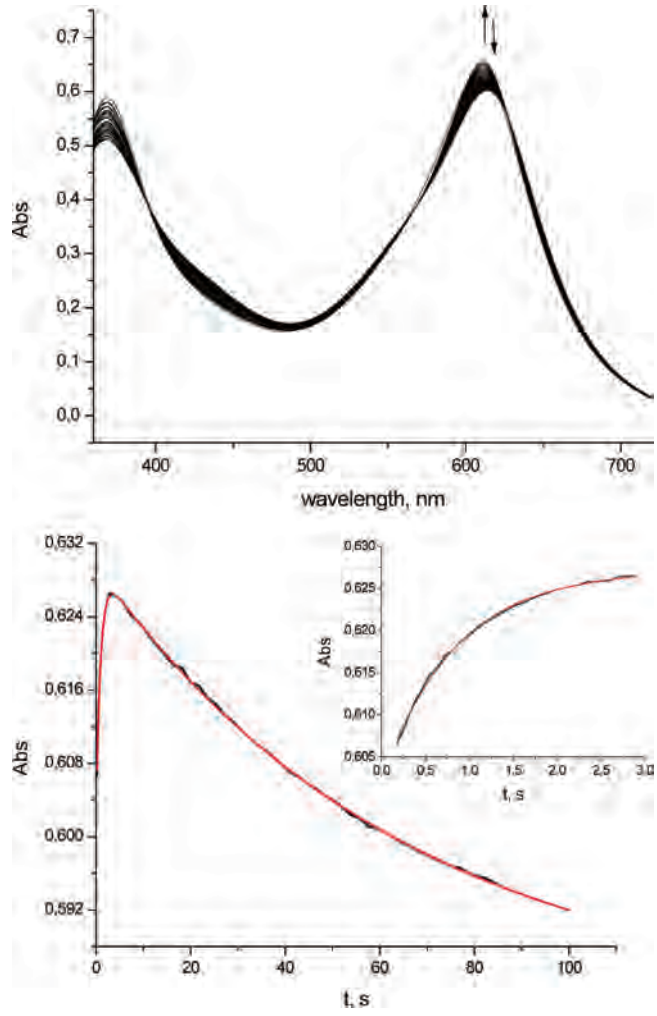

Figure 11. Typical spectral changes and the kinetic trace for the direct reaction with H_2O_2. $[Fe^{III}(Pz)] = 3 \times 10^{-5}$ M, $[H_2O_2] = 6 \times 10^{-4}$ M, pH = 12, T = 3 °C, and μ = 0.2 M ($NaClO_4$).

the concentration of the catalyst is 10^{-6} M, only ~30% of Orange II is oxidized, which is 0.3 × 10^{-4} M. This concentration is still 30 times larger than the initial concentration of the catalyst, which clearly shows that the reaction is not stoichiometric but catalytic. At the end of the fast reaction, a second slower step occurs. The reason for the incomplete oxidation of Orange II is ascribed to the inactivation of the catalyst during the oxidation process, i.e., parallel destruction of $Fe^{III}(Pz)$. The subsequent slow reaction is likely catalyzed by traces of iron(III) produced during the destruction $Fe^{III}(Pz)$. Products like $OH^{\bullet}$ formed during homolysis of H_2O_2 by iron(III) could lead to the further oxidation of Orange II as well as the inactivation of the catalyst. Complete oxidation of Orange II occurs at a catalyst concentration higher than 4 × 10^{-6} M. The data reported for the direct reaction of $[Fe^{III}(Pz)(H_2O)]^{7-}$ with hydrogen peroxide indi-

Scheme 11. Proposed Reaction Scheme for the Formation of $[Fe(Pz)(OH)(OOH)]^{9-}$ at pH = 12

$$[Fe(Pz)(OH)(H_2O)]^{8-} \rightleftharpoons [Fe(Pz)(OH)_2]^{9-} + H^+ \qquad K_{a2}$$

$$[Fe(Pz)(OH)(H_2O)]^{8-} + HOO^- \rightleftharpoons [Fe(Pz)(OH)(OOH)]^{9-} + H_2O \qquad k_{on}, k_{off}, K$$

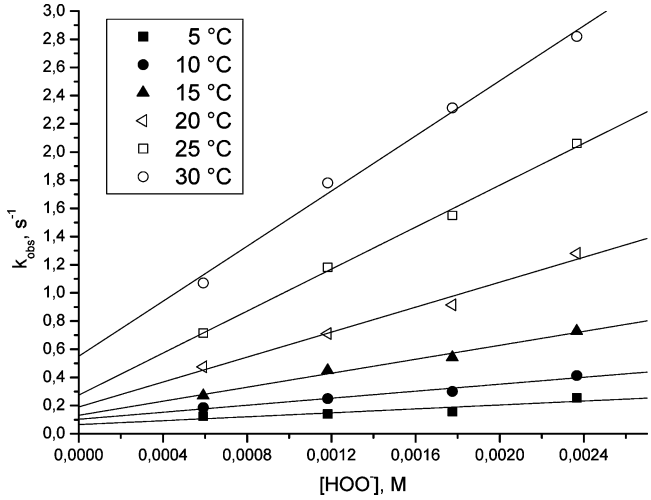

Figure 12. Concentration dependence of k_{obs} for the direct reaction with H_2O_2 and the corresponding linear fits. $[Fe^{III}(Pz)(OH)_2]^{9-}] = 3 \times 10^{-5}$ M, pH = 12, and $\mu = 0.2$ M ($NaClO_4$).

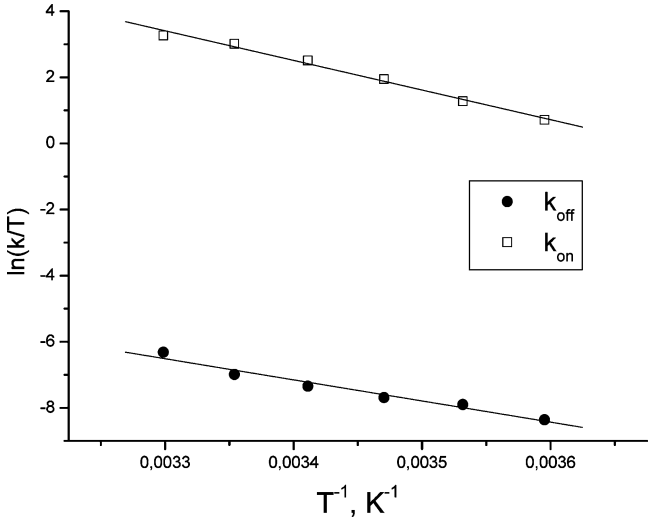

Figure 13. Eyring plots for the direct reaction of hydrogen peroxide with $Fe^{III}(Pz)$ at pH = 12. The k_{on} and k_{off} values were obtained from the linear fits of the peroxide concentration dependence in Figure 12. $[Fe^{III}(Pz)(OH)_2]^{9-}] = 3 \times 10^{-5}$ M, pH = 12, and $\mu = 0.2$ M ($NaClO_4$).

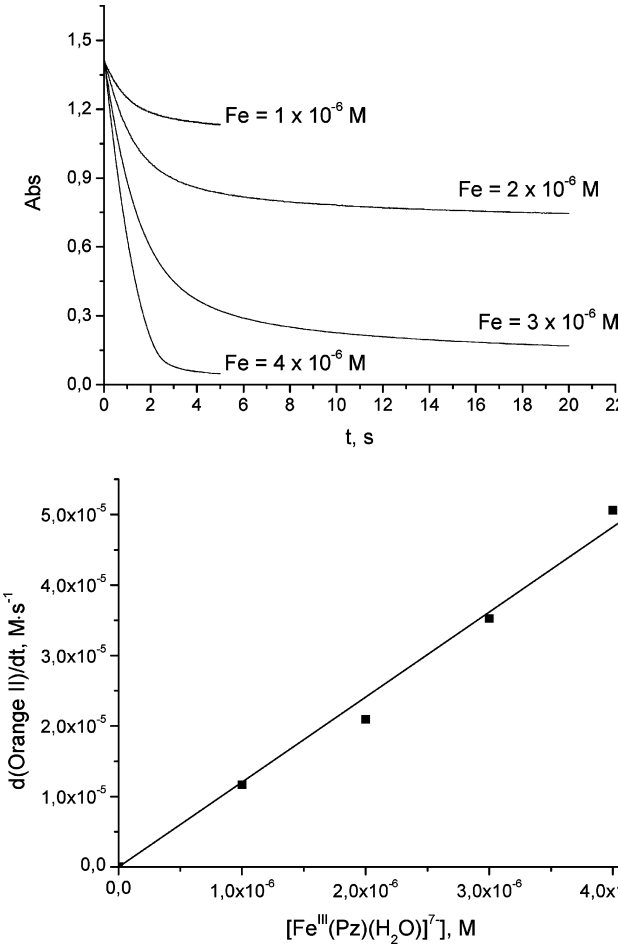

Figure 14. Decomposition of Orange II by H_2O_2 in the presence of $[Fe^{III}(Pz)(H_2O)]^{7-}$ and the dependence of the initial reaction rate on the Fe^{III} concentration. $[H_2O_2] = 0.025$ M, $[Fe^{III}(Pz)] = (1–4) \times 10^{-6}$ M, [Orange II] $= 1 \times 10^{-4}$ M, pH = 3, $T = 25$ °C, and $\mu = 0.1$ M ($NaClO_4$).

cated decomposition of the catalyst in the absence of a substrate, which now occurs as a competing parallel reaction.

The kinetic data can also be interpreted in a quantitative way. The initial rate of the oxidation process depends linearly on the concentration of $Fe^{III}(Pz)$ and H_2O_2 (see Figures 14 and 15, respectively, and Table S10 in the Supporting Information). The slopes of the linear fits were found to be 12.06 ± 0.07 and $(2.09 \pm 0.01) \times 10^{-3}$ s^{-1}, respectively. This is consistent with a mechanism involving coordination of the peroxide to the Fe center and transformation of the peroxo complex into the catalytic species. The dependence of the rate of the reaction on the Orange II concentration shows an unexpected inverse dependence (see Figure 16). This shows that higher Orange II concentrations inhibit the reaction. If the inverse initial rate is plotted against the Orange II concentration, a linear dependence is observed. The slope and intercept of the linear fit were found to be $(6.75 \pm 0.05) \times 10^7$ s M^{-2} and $(2.65 \pm 0.04) \times 10^4$ s M^{-1}, respectively. To account for this observation, we suggest that Orange II can partially coordinate to, or form an adduct with, $Fe^{III}(Pz)$, which hinders the activation of hydrogen peroxide. These observations can be accounted for in terms of the reactions outlined in Scheme 12, where $Fe^{III}(Pz)$ represents $[Fe^{III}(Pz)(H_2O)]^{7-}$ at pH = 3. The suggested overall catalytic cycle is presented in Scheme 13.

On the basis of Scheme 12, rate law (7) can be derived (see the Supporting Information), which accounts for the decrease in the reaction rate with increasing Orange II concentration.

$$-\frac{d[ORII]}{dt} = \frac{k_3K_2[H_2O_2][Fe^{III}(Pz)]_T}{1 + K_1[ORII] + K_2[H_2O_2]} \quad (7)$$

The concentration dependence of the Orange II decomposition rate on $[H_2O_2]$ is linear. Because no curvature is observed, eq 7 can be simplified to eq 8,

$$-\frac{d[ORII]}{dt} = \frac{k_3K_2[H_2O_2][Fe^{III}(Pz)]_T}{1 + K_1[ORII]} \quad (8)$$

which can be rewritten as

$$-\frac{dt}{d[ORII]} = \frac{1}{rate} = \frac{1}{k_3K_2[H_2O_2][Fe^{III}(Pz)]_T} + \frac{K_1[ORII]}{k_3K_2[H_2O_2][Fe^{III}(Pz)]_T} \quad (9)$$

From the slope and intercept of the linear fit in Figure 16, K_1 (=slope/intercept in eq 9) could be calculated to be 2547 ± 18 M^{-1}. From the slopes of the linear fits in Figures 14 and 15, the term k_3K_2 could be calculated and was found to be 605 ± 10 and 656 ± 9 M^{-1} s^{-1}, respectively. From the slope as well as from the intercept of the linear fit in Figure 16 using eq 8, k_3K_2 was found to be 754 ± 5 M^{-1} s^{-1}. The average value of k_3K_2 is therefore 670 ± 70 M^{-1} s^{-1} at 25 °C.

Catalytic Decomposition of Orange II by H_2O_2 in the Presence of $[Fe^{III}(Pz)(H_2O)(OH)]^{8-}$. At pH = 10, the aquahydroxo complex is the dominant species present in solution. Typical spectral changes and kinetic traces as a function of the catalyst and H_2O_2 concentrations observed under these conditions are reported in Figures 17 and 18 (and Figure S18 and Table S11 in the Supporting Information). The kinetic traces exhibit typical zero-order kinetics and the reaction rate depends linearly on both the catalyst and H_2O_2 concentrations. The slopes of the linear fits were found to be 0.61 ± 0.02 and (3.12 ± 0.03) × 10^5 s^{-1}, respectively. The formation of the catalytically active species is expected to include the fast coordination of peroxide, followed by the cleavage of the O−O bond either heterolytically (formation of OH^- and $(Pz^{\bullet+})Fe^{IV}$=O) or homolytically (formation of $OH^{\bullet}$ and $(Pz)Fe^{IV}$=O). The latter reaction is expected to be the rate-determining step. The dependence on the Orange II concentration was also studied under these conditions (see Figure 19). The reaction again slows down upon an increase of the Orange II concentration, and the inverse initial rate depends linearly on the Orange II concentration, similar to the experiments at pH = 3. The slope and intercept of the fit were found to be (1.37 ± 0.02) × 10^9 s M^{-2} and (6.28 ± 0.03) × 10^5 s M^{-1}, respectively. From these data, K_1 could be calculated (in the same way as shown above) to be 2181 ± 34 M^{-1}, which is in close

Scheme 12. Proposed Reaction Scheme for the Catalyzed Oxidation of Orange II

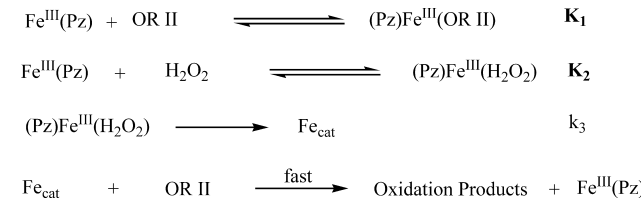

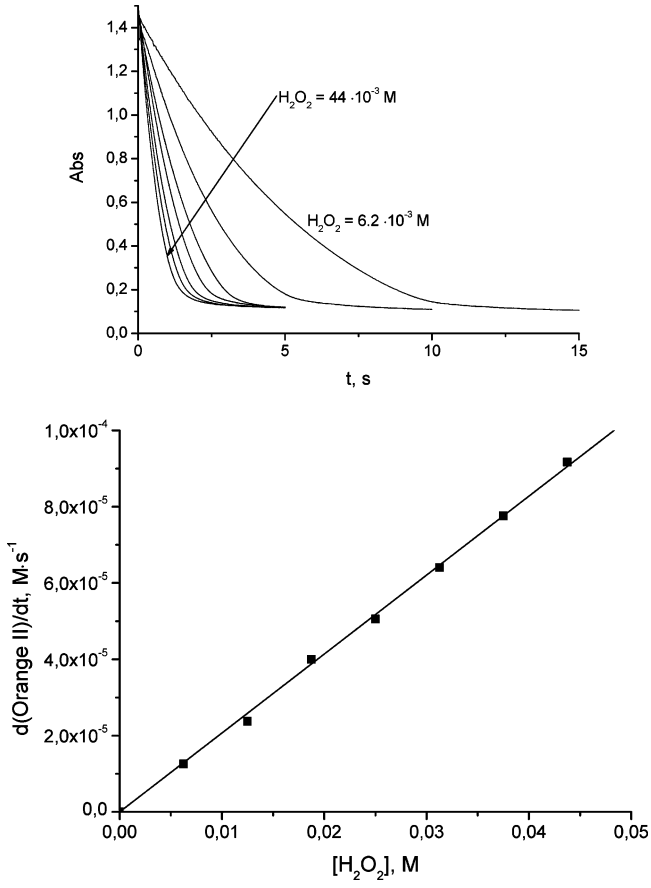

Figure 15. Decomposition of Orange II by H_2O_2 in the presence of $[Fe^{III}(Pz)(H_2O)]^{7-}$ and the dependence of the initial reaction rate on the H_2O_2 concentration. $[H_2O_2]$ = (6.2–44) × 10^{-3} M, $[Fe^{III}(Pz)]$ = 4 × 10^{-6} M, [Orange II] = 1 × 10^{-4} M, pH = 3, T = 25 °C, and μ = 0.1 M ($NaClO_4$).

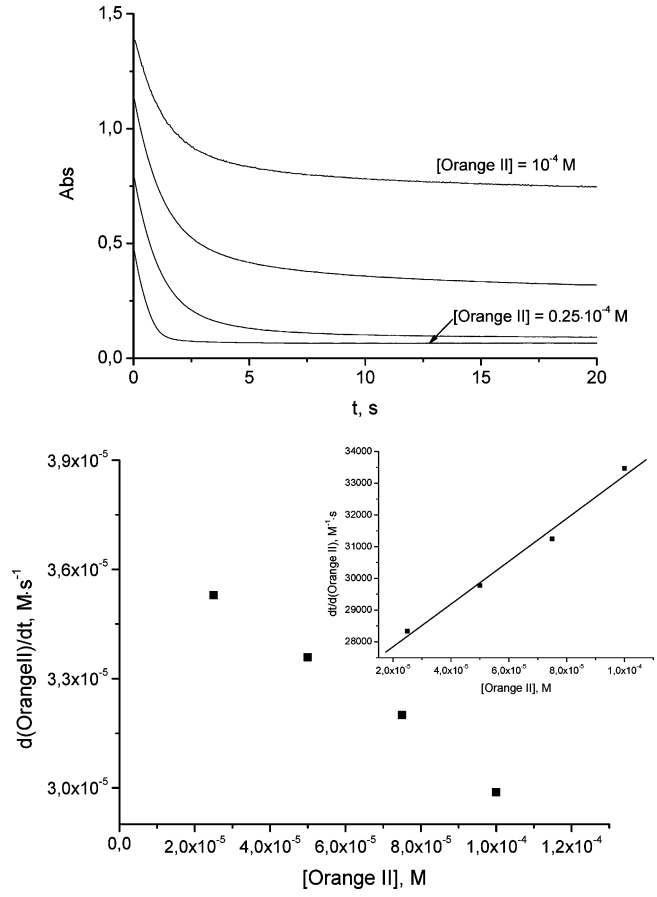

Figure 16. Decomposition of Orange II by H_2O_2 in the presence of $[Fe^{III}(Pz)(H_2O)]^{7-}$ and the dependence of the initial reaction rate and the inverse rate (inset) on the Orange II concentration. $[H_2O_2]$ = 0.025 M, $[Fe^{III}(Pz)]$ = 2 × 10^{-6} M, [Orange II] = 1 × 10^{-4} M, pH = 3, T = 25 °C, and μ = 0.1 M ($NaClO_4$).

Scheme 13. Proposed Mechanism for the Oxidation of Orange II by H_2O_2 in the Presence of $[Fe^{III}(Pz)(H_2O)]^{7-}$ at pH = 3[a]

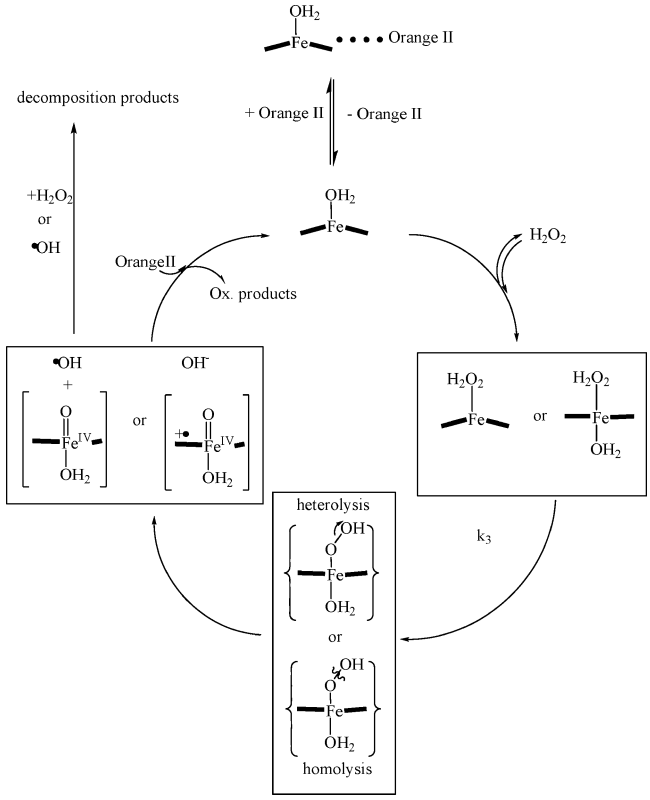

[a] The proposed intermediate may not be six-coordinate.

agreement with the value found at pH = 3. This means that also under these conditions Orange II can inhibit the catalytic activity of the catalyst, as suggested in Scheme 12, where $Fe^{III}(Pz)$ represents $[Fe^{III}(Pz)(H_2O)(OH)]^{8-}$ at pH = 10. The suggested overall catalytic cycle is presented in Scheme 14.

The rate data in Figures 17−19 can be used to determine the value of k_3K_2 at pH = 10 using eqs 8 and 9. From the intercept of the linear fit in Figure 19, k_3K_2 was found to be 13.63 ± 0.01 M^{-1} s^{-1}. From the slopes of the linear fits in Figures 17 and 18, k_3K_2 was calculated to 12.7 ± 0.1 and 19.00 ± 0.02 M^{-1} s^{-1}, respectively, such that the average value of k_3K_2 is 15 ± 3 M^{-1} s^{-1} at 25 °C.

Catalytic Decomposition of Orange II by H_2O_2 in the Presence of $[Fe^{III}(Pz)(OH)_2]^{9-}$. In very alkaline solutions (pH = 13), no catalytic oxidation was observed. The dihydroxo form of the $Fe^{III}(Pz)$ complex seems to be totally inactive. The reason for this behavior is the inability of the hydroperoxide ion to displace the strongly coordinated hydroxyl ligands. We performed some experiments at pH = 12, where the more labile form of the catalyst, i.e., $[Fe^{III}(Pz)(H_2O)(OH)]^{8-}$, is present at ca. 12% in solution and accounts for the observed catalytic activity. The results in Figures 20 and 21 (and Table S12 in the Supporting Information) show the dependencies of the initial reaction rate on the concentration of HOO^- and $Fe^{III}(Pz)$, respectively. The hydroperoxide ion has a much higher nucleophilicity than H_2O_2, which leads to a more efficient formation of $[Fe^{III}(Pz)(OH)(OOH)]^{9-}$ via substitution of coordinated water by HOO^-. This, in turn, is responsible for the nonlinear

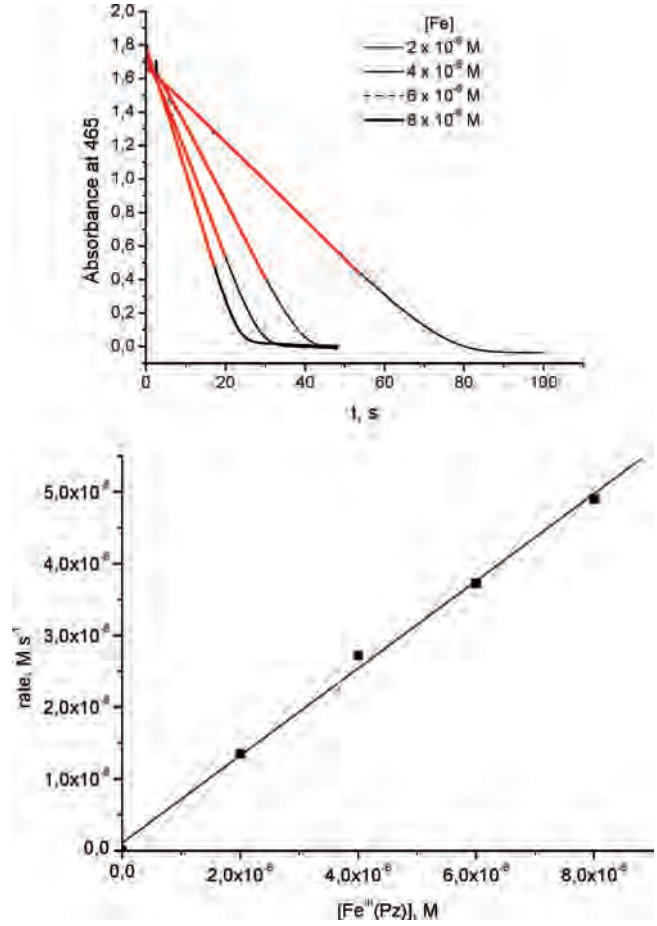

Figure 17. Kinetic traces and plot of the reaction rate for the catalyzed decomposition of Orange II as a function of the $Fe^{III}(Pz)$ concentration. [Orange II] = 1 × 10^{-4} M, $[H_2O_2]$ = 0.0584 M, T = 25 °C, μ = 0.2 M ($NaClO_4$), and pH = 10 (CAPS buffer).

dependence of the initial rate on the H_2O_2 concentration shown in Figure 20. On the basis of a combination of Schemes 11 and 12 (where $Fe^{III}(Pz)$ now represents $[Fe^{III}(Pz)(H_2O)(OH)]^{8-}$), rate law (7) modifies to (10) in order to account for the fraction of the reactive aquahydroxo complex present at this pH. Under such conditions, K_2 in Scheme 12 equals K in Scheme 11, i.e., (2.2 ± 0.5) × 10^4 M^{-1}.

$$-\frac{d[ORII]}{dt} = \frac{k_3K[HOO^-][Fe^{III}(Pz)]_T}{\frac{K_{a_2}}{[H^+]} + 1 + K_1[ORII] + K[HOO^-]} \quad (10)$$

Equation 10 can be rewritten as shown in eq 11,

$$-\frac{dt}{d[ORII]} = \frac{\frac{K_{a_2}}{[H^+]} + 1 + K_1[ORII]}{k_3K[HOO^-][Fe^{III}(Pz)]_T} + \frac{1}{k_3[Fe^{III}(Pz)]_T} \quad (11)$$

according to which the double reciprocal plot in the lower diagram of Figure 20 was constructed. The slope and intercept were found to be 244 ± 12 s and (9.4 ± 1.0) × 10^4 s M^{-1}, respectively. From the slope of the line (slope = $1/k_3[Fe]_T$), k_3 was found to be 1.1 ± 0.1 s^{-1} at 25 °C. From

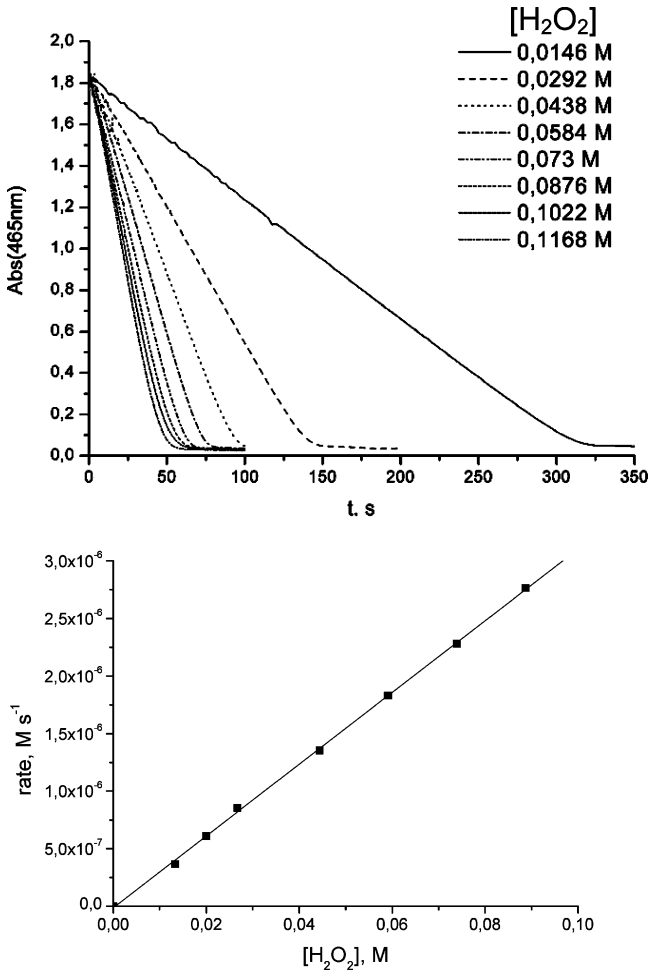

Figure 18. Kinetic traces and plot of reaction rate for the catalyzed decomposition of Orange II as a function of the H_2O_2 concentration. [Orange II] = 1×10^{-4} M, [Fe^{III}(Pz)] = 2×10^{-6} M, T = 25 °C, μ = 0.2 M ($NaClO_4$), and pH = 10 (CAPS buffer).

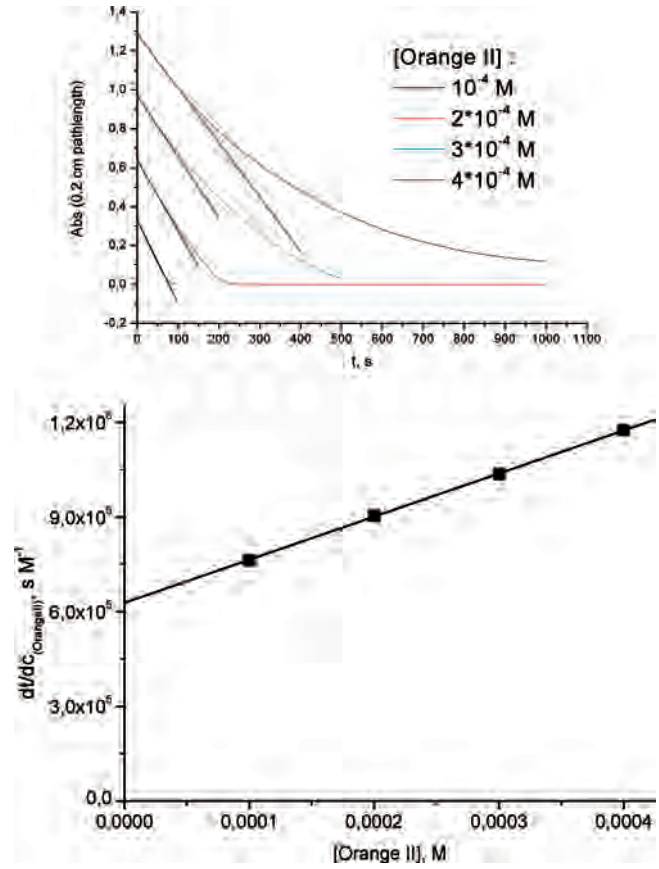

Figure 19. Effect of the Orange II concentration on the initial reaction rate. In the second diagram, the values of the reciprocal rates are plotted versus the concentration of Orange II. T = 25 °C, [H_2O_2] = 0.0584 M, [Fe^{III}(Pz)(OH_2)OH^{8-}] = 2×10^{-6} M, and pH = 10 (CAPS buffer).

the slope/intercept for eq 11, K_1 could be calculated because K is known from the direct reaction of peroxide with Fe^{III}(Pz) at this pH. K_1 was found to be $(5.1 \pm 1.1) \times 10^5$ M^{-1} at 25 °C.

These results are in line with that expected on the basis of Michaelis–Menten kinetics, as expressed by eq 7. Furthermore, we measured the initial rate of the reaction as a function of the pH under the same conditions, i.e., constant catalyst, peroxide, and Orange II concentrations. Figure 22 reports the dependence of the initial rate on the pH. As expected, lower reaction rates are observed at pH = 10, where the peroxide molecule is present in the fully protonated form. The maximum rate is observed at pH = 11, where enough hydroperoxide and the aquahydroxo form of the catalyst are present in solution. Upon a further increase in the pH of the solution, smaller amounts of the active catalyst are present and the reaction rate decreases until there is no catalytic activity anymore at very alkaline pH. What is the importance of the deprotonation of Orange II at alkaline pH (Figure S1 in the Supporting Information)? This does not seem to play an important role in terms of the easiness of oxidation because the inactivation of the catalyst leads to a decrease in the reaction rate. Therefore, even if Orange II was easier to oxidize in its deprotonated form, there is no active catalyst to activate peroxide and initiate the catalytic cycle. The observed slow decomposition at very high pH is not ascribed to a catalytic reaction but rather to the direct reaction of Orange II with $OH^{\bullet}$ radicals generated from peroxide at this pH. However, as demonstrated by the simulations presented in the next section, the inhibition of catalytic activity due to coordination of the deprotonated Orange II to Fe^{III}(Pz) is clearly visible.

Simulation of Kinetic Traces. The reported results demonstrate that the underlying chemistry of the Fe^{III}(Pz)/H_2O_2/Orange II system is rather complex. The kinetic traces are not those usually observed during a reaction and cannot be fitted with a single- or double-exponential fit. The reported kinetic data form the basis for the proposed mechanism given above. To what extent can the suggested mechanism account for the observed kinetic traces? Simulations of the experimental traces were performed to prove the proposed reaction scheme. For this purpose, we used the program *Pro-KII*[36] to fit and simulate the kinetic data.

The ideal pH range to simulate the observed kinetic traces is pH = 10. Following a short induction period, a zero-order reaction is visible and the maximum rate of this reaction is the rate used in the concentration-dependent plots. The kinetic traces were imported into the program along with

(36) *Pro-KineticistII*, version 1.08; Applied Photophysics Ltd.: Leatherhead, England, 2001.

Scheme 14. Proposed Mechanism for the Overall Oxidation of Orange II by H_2O_2 in the Presence of $[Fe^{III}(Pz)(H_2O)(OH)]^{8-}$ at pH = 10

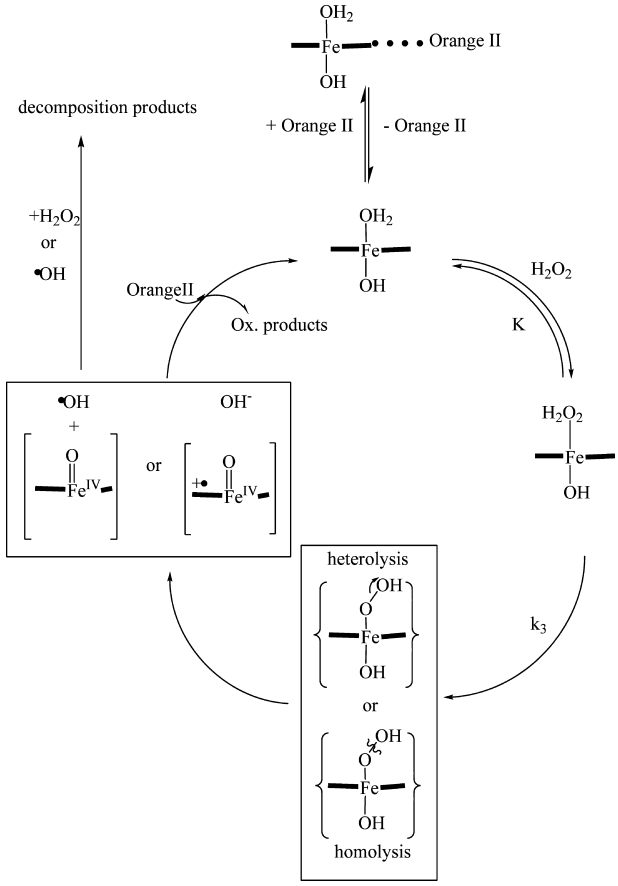

the proposed reaction scheme shown in Scheme 11. The value of K_1 used to simulate the data was 2×10^3 M^{-1}. The simulated trace perfectly fits the experimental one, as shown in Figure 23. However, to test the model, we also selected traces at other experimental conditions, i.e., at different $[Fe^{III}(Pz)]$ and H_2O_2 concentrations, as shown in Figure 23. The simulated value found for k_3K_2, viz., 23.0 ± 0.2 M^{-1} s^{-1}, is close to that found experimentally (average value = 15 ± 3 M^{-1} s^{-1}). The simulated constants $k_3 = 2.3$ s^{-1} and $K_2 = 10$ M^{-1} are in reasonable agreement with the experimental values given above.

At pH = 12, we could also simulate the kinetic traces as shown in Figure 24. Because the value of K_2 was measured directly at this pH, it was used as a fixed value in the simulation. The constant k_3 was found to be 1.2 s^{-1}. K_1 was found to be 6×10^5 M^{-1}, which is 300 times larger than that found at pH = 10. This means that deprotonation of Orange II, favored by increasing pH, leads to a stronger inhibition of the catalytic reaction. Efforts to fit the kinetic traces for acidic pH were not as successful. The reason for this is the parallel spontaneous decomposition reaction of the catalyst. If this is included into the kinetic scheme, it affects the results for the extracted rate and equilibrium constants.

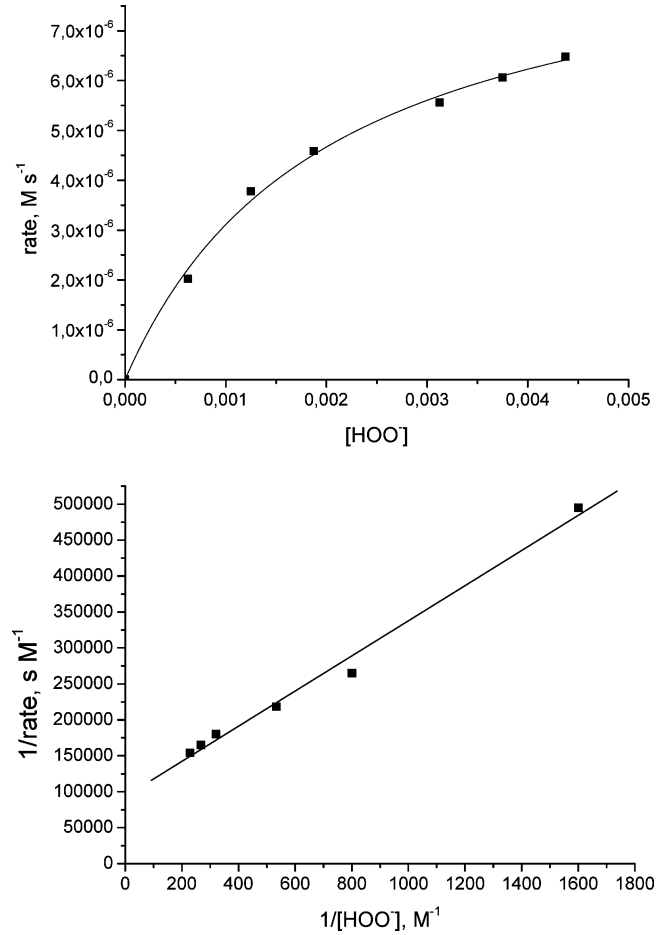

Figure 20. Dependence of the reaction rate on the HOO^- concentration. pH = 12, $[Fe^{III}(Pz)] = 10^{-5}$ M, [Orange II] = 1×10^{-4} M, $T = 25$ °C, and $\mu = 0.2$ M ($NaClO_4$). The lower plot shows the Michaelis–Menten linearization.

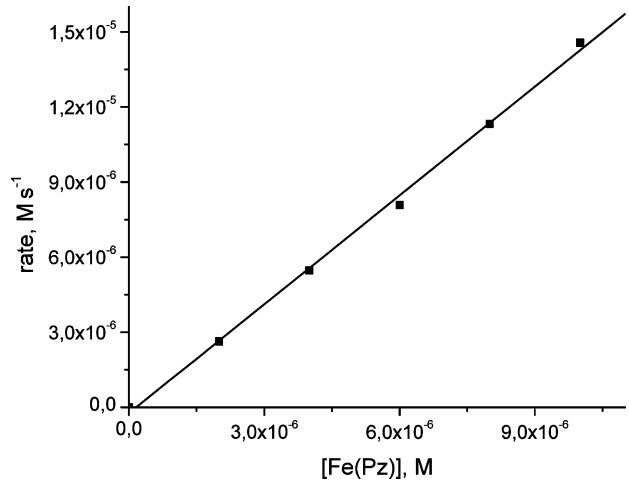

Figure 21. $Fe^{III}(Pz)$ concentration dependence of the initial reaction rate. pH = 12, $[H_2O_2] = 0.026$ M, [Orange II] = 1×10^{-4} M, $T = 25$ °C, and $\mu = 0.2$ M ($NaClO_4$).

Conclusions

The speciation of $Fe^{III}(Pz)$ as a function of the pH was extensively studied. At acidic pH, $[Fe^{III}(Pz)(H_2O)]^{7-}$ is the dominant species, which is in equilibrium with the diaqua species. This was concluded from theoretical calculations as well as from the temperature and pressure dependence of

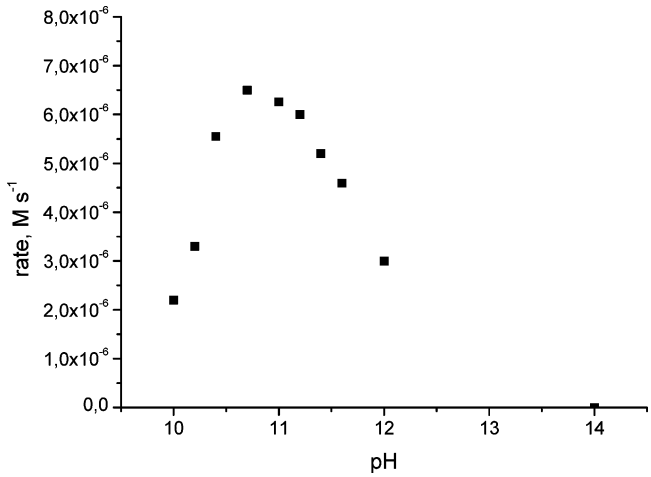

Figure 22. pH dependence of the initial reaction rate. The initial slopes of the kinetic traces were divided by the ϵ value of Orange II at every pH (see Figure S1 in the Supporting Information) to convert these to reaction rates. $[Fe^{III}(Pz)] = 2 \times 10^{-6}$ M, $[H_2O_2] = 0.058$ M, $T = 25$ °C, and $\mu = 0.2$ M ($NaClO_4$)

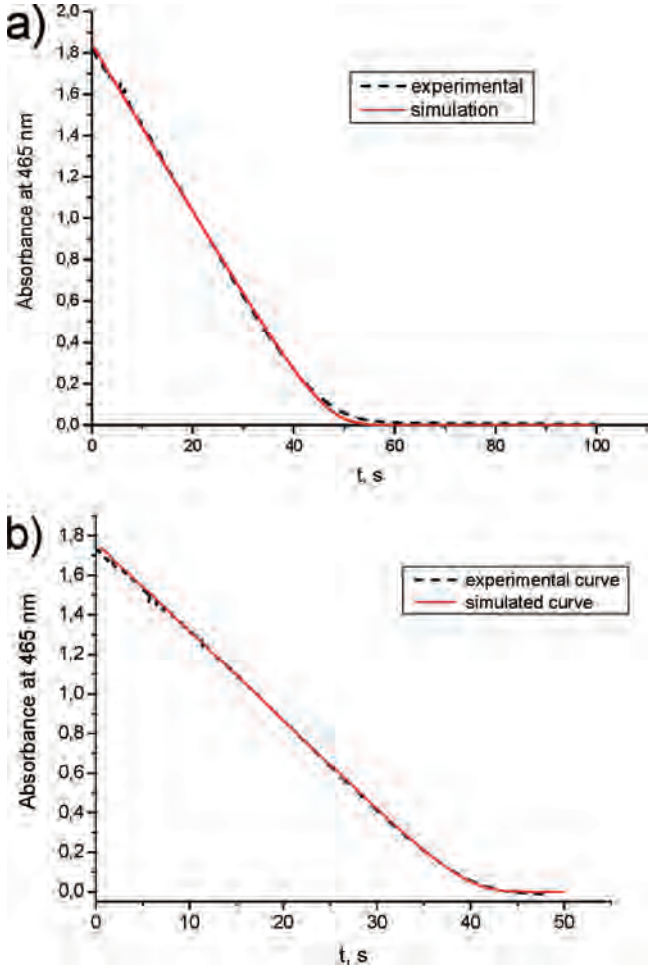

Figure 23. Simulation of the kinetic traces at pH = 10. The following experimental conditions were used: (a) $[Fe^{III}(Pz)] = 4 \times 10^{-6}$ M, $T = 25$ °C, $\mu = 0.2$ M, $[H_2O_2] = 0.0584$ M, [Orange II] = 10^{-4} M; (b) $[Fe^{III}(Pz)] = 2 \times 10^{-6}$ M, $T = 25$ °C, $\mu = 0.2$ M, $[H_2O_2] = 0.118$ M, [Orange II] = 10^{-4} M. Constants used in the simulation: log $K_2 = 3.32$, log $K_1 = 1$, $k_3 = 2.31$ s^{-1}.[36]

the UV–vis spectra at this pH. This species is red and Fe^{III} is in the intermediate-spin state. Increasing the pH results in

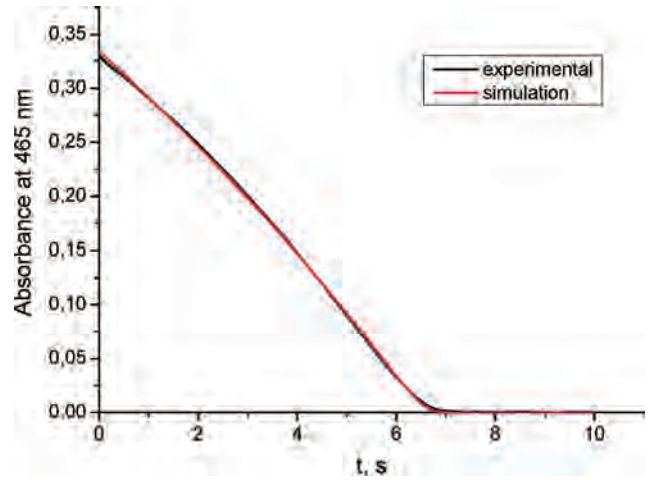

Figure 24. Simulation of the kinetic trace at pH = 12. The following experimental conditions were used: $[Fe^{III}(Pz)] = 1 \times 10^{-5}$ M, pH = 12, $T = 25$ °C, $\mu = 0.2$ M, $[H_2O_2] = 31.25 \times 10^{-4}$ M, [Orange II] = 10^{-4} M. Constants used in the simulation: log $K_1 = 5.78$, log $K_2 = 4.34$, $k_3 = 1.2$ s^{-1}.[36]

the axial coordination of a hydroxide ligand to the Fe^{III} center and changes the spin state to low spin ($pK_{a_1} = 7.50 \pm 0.02$). This is accompanied by large spectral changes, and the solution becomes blue. The water exchange reaction, which was measurable at pH = 1, now becomes very fast. A further increase in the pH results in the formation of the dihydroxo complex $[Fe^{III}(Pz)(OH)_2]^{9-}$ ($pK_{a_2} = 11.16 \pm 0.06$). The reactions with NO were also studied for this complex as a function of the pH. Upon the addition of NO, reduction of the Fe center occurs and $Fe^{II}NO^+$ is produced.

On the basis of the obtained mechanistic information, the activation of hydrogen peroxide by this complex was studied. The direct reaction of H_2O_2 with $Fe^{III}(Pz)$ is always very fast and controlled by the water exchange reaction. The catalyzed oxidation of Orange II shows large differences as a function of the pH. At acidic pH, the oxidation is not complete at low catalyst concentrations, whereas at higher pH, a zero-order kinetic trace is observed and the oxidation of Orange II always goes to completion. The different reactive species of $Fe^{III}(Pz)$ and H_2O_2 at each pH play an important role in terms of the generation of the catalytic species, which is demonstrated by the pH dependence of the reaction. The results at pH = 3, although reported only quantitatively, show the pattern followed by this reaction. There are side reactions (such as decomposition of the catalyst) that were not taken into account during the quantitative interpretation. At pH = 10 and 12, however, the experimental results could be simulated with the suggested catalytic mechanism, demonstrating the general applicability of the proposed catalytic cycle. Further mechanistic details could be revealed by the activation parameters determined from the temperature and pressure dependence of the individual reaction steps.

Table 1 summarizes the values for the term k_3K_2 at each pH, which was determined experimentally and by simulation of the kinetic traces. The lowest value for this term is the one found for pH = 10. Increasing the pH to 12 accelerates the catalytic reaction. This can be interpreted in terms of

Table 1. Experimental and Simulated Values for K_1, K_2, and k_3 as a Function of the pH

	pH = 3	pH = 10	pH = 12
K_1(exp), M^{-1}	2547 ± 18	2181 ± 14	(5.1 ± 1.1) × 10^5
K_1(sim), M^{-1}		2089	6 × 10^5
K_2(exp), M^{-1}			(2.2 ± 0.5) × 10^4
K_2(sim), M^{-1}		10	2.2 × 10^4
k_3(exp), s^{-1}			1.1 ± 0.1
k_3(sim), s^{-1}		2.3	1.2
K_2k_3(exp), M^{-1} s^{-1}	670 ± 70	15 ± 3	(2.4 ± (0.6) × 10^4
K_2k_3(sim), M^{-1} s^{-1}		23.0 ± 0.2	2.6 × 10^4

the deprotonation of hydrogen peroxide, which leads to a much stronger nucleophile. Therefore, the value for K_2 is approximately 2000 times higher. The reactive species of the porphyrazine complex is the same at pH = 10 and 12, viz., $[(Pz)Fe(OH)(H_2O)]^{8-}$. Decreasing the pH to 3 also accelerates the reaction, although the acceleration factor is now 30. If we assume that K_2 at pH = 3 is between 10 and 20 M^{-1}, then k_3 is in the range 30−60 s^{-1}. This is consistent with acid-catalyzed heterolytic cleavage of the O−O bond, which is the rate-determining step of the reaction.[5] The equilibrium constant K_1 also shows large differences (see Table 1) and is approximately (1–2) × 10^3 times higher at pH = 12 than at pH = 10 and 3. This can be accounted for in terms of the deprotonation of Orange II (see Figure S1 in the Supporting Information). From the values of K_1 at each pH, we can expect K_2 to also have similar values at pH = 3 and 10 because K_2 represents the equilibrium constant for a complex formation reaction similar to K_1.

In the case of iron(III) porphyrin complexes, catalytic intermediates have been fully characterized.[5] Our results show that the $Fe^{III}(Pz)$ complex can act as an effective catalyst in oxidation reactions especially at higher pH. A comparison of our kinetic results with those in the literature for the porphyrin complexes shows close similarities in the reactivity of the macrocycles. Further mechanistic investigations and product characterization are therefore important because similar intermediates are expected to be produced. Such studies should be performed in nonaqueous solutions where high-valent $(Pz^{\bullet+})Fe^{IV}{=}O$ species will be more stable and easier to characterize.

Acknowledgment. The authors gratefully acknowledge financial support from the Deutsche Forschungsgemeinschaft within SFB 583 "Redox-active metal complexes". The simulations were performed on a test version of the program *Pro-KII*, which was kindly supplied by Applied Photophysics.

Supporting Information Available: Tables S1−S11, Figures S1−S18, and derivation of the rate law for the decomposition of Orange II. This material is available free of charge via the Internet at http://pubs.acs.org.

IC702041G